NUCLEAR MAGNETIC RESONANCE BASED CHARACTERIZATION OF THE PROTEIN BINDING POCKET USING HYPERPOLARIZED LIGAND

A Thesis

by

HLAING ZAYAR MIN

Submitted to the Office of Graduate and Professional Studies of
Texas A&M University
in partial fulfillment of the requirements for the degree of

MASTER OF SCIENCE

Chair of Committee,	Christian Hilty
Committee Members,	Emile Schweikert
	Li Liu
Head of Department,	David H. Russell

August 2014

Major Subject: Chemistry

ABSTRACT

In the drug design process, the structural determination of the protein-ligand binding interface and understanding how the drug binds to the target protein at the protein binding pocket is essential. In the past few years, Dynamic Nuclear Polarization (DNP) combined with Nuclear Magnetic Resonance (NMR) has emerged as a new tool for studying interactions between different molecules. In this study, the DNP-NMR technique was employed for characterization of the protein binding pocket through binding of the hyperpolarized ligand to the protein. Trypsin and benzamidine were chosen as models for the protein and the ligand because the binding of benzamidine to trypsin is well-known.

Several enhanced NMR signals of trypsin appeared from the binding of hyperpolarized benzamidine to trypsin. A significant finding was that those trypsin signals were non-uniformly enhanced when compared with the trypsin signals in the conventional (non-hyperpolarized) NMR spectrum, suggesting that a specific region of the protein, most likely the protein-binding pocket proximal to the bound hyperpolarized ligand, is selectively polarized. The polarization transfer process was described mathematically by fitting model equations to the enhanced signal intensities of both the protein and the ligand. A fit parameter was evaluated, which assuming the presence of a single spin on protein and ligand can be interpreted as a cross-relaxation rate (σ_{DNP}), that can provide spatial information between the two spins.

Saturation Transfer Difference (STD)-NMR was employed as an independent method to measure the protein-ligand interaction. The fit parameters in the STD-NMR equations, the dissociation constant (K_D) and a cross-relaxation rate (σ_{STD}), were evaluated. K_D determined from STD-NMR was consistent with the K_D values reported in the literatures, suggesting that STD-NMR data is reliable. σ_{STD} evaluated from STD-NMR was compared with σ_{DNP} evaluated from the DNP-NMR and found to be similar in magnitude.

ACKNOWLEDGEMENTS

I would like to thank my advisor, Dr. Hilty, and my committee members, Dr. Schweikert and Dr. Liu, for their guidance and support throughout the course of this academic journey.

I also want to extend my gratitude to the contributors of this project: Haifeng Zeng (past group member), Giridhar Sekar and Youngbok Lee (past group member).

Thanks also go to my group members, friends and colleagues and the department faculty and staff for making my time at Texas A&M University a fabulous experience.

NOMENCLATURE

NMR	Nuclear Magnetic Resonance
DNP	Dynamic Nuclear Polarization
STD	Saturation Transfer Difference
3D	Three Dimensional
kDa	Kilo Daltons
NOE	Nuclear Overhauser Effect
CIDNP	Chemically Induced Dynamic Nuclear Polarization
OP	Optical Pumping
PHIP	Parahydrogen Induced Polarization
DMSO	Dimethyl Sulfoxide
TEMPOL	4-hydroxy-2,2,6,6-tetramethylpiperidine-1-oxyl
UV	Ultraviolet
ICT	Isothermal Calorimetric Titration
K_D	Dissociation Constant

TABLE OF CONTENTS

Page

ABSTRACT ii

ACKNOWLEDGEMENTS iv

NOMENCLATURE v

TABLE OF CONTENTS vi

LIST OF FIGURES viii

LIST OF TABLES ix

1. INTRODUCTION 1

1.1 Sensitivity of NMR 2
1.2 Theoretical background on DNP 3
1.3 DNP-NMR methods for study of chemical and biological systems 6
1.4 Nuclear Overhauser Effect (NOE) 7
1.5 Saturation Transfer Difference NMR (STD-NMR) 11

2. EXPERIMENTAL METHODS 15

2.1 DNP-NMR experimental setup and method 15
2.2 DNP-NMR pulse program 19
2.3 DNP-NMR spectra and data processing 20
2.4 STD-NMR pulse program 21

3. RESULTS AND DISCUSSION 22

3.1 Selectively enhanced NMR resonances in DNP-NMR 22
3.2 Comparison of the DNP-NMR and STD-NMR spectrum 24
3.3 Analysis of different peaks in STD-NMR 27
3.4 Signal buildup in the time-resolved DNP-NMR spectra 29
3.5 Evaluation of the cross-relaxation rate (σ_{DNP}) in DNP-NMR 34
3.6 Analysis of STD-NMR data 36
3.7 Determination of spin-lattice relaxation time (T_1) 40
3.8 Evaluation of STD-NMR data 43

3.9 Determination of K_D with Isometric Calorimetric Titration (ICT) 48
3.10 Comparison between DNP-NMR and STD-NMR 50

4. SUMMARY AND CONCLUSION 51

REFERENCES 54

LIST OF FIGURES

FIGURE		Page
1	Scheme illustrating solid effect DNP	5
2	Energy level diagram showing spin populations in a two spin system	7
3	Relaxation pathways in an irradiated two spins system	8
4	Illustration of the STD-NMR experiment	12
5	DNP-NMR pulse sequence	19
6	Mathematically defined baseline for the peak	20
7	1D stacked proton NMR spectra from the DNP-NMR experiment	23
8	Comparison of trypsin spectrum from different experiments	25
9	STD signal at different saturation frequencies	28
10	Polarization signal of trypsin and benzamidine in DNP experiment	30
11	Proton signal build-up for different enhanced peaks	35
12	Determination of T_1(s) for pure benzamidine in H_2O solvent	40
13	Determination of T_1(s) for pure benzamidine in D_2O solvent	41
14	Determination of T_1(s) for trypsin in H_2O solvent	42
15	Determination of T_1(s) for trypsin in D_2O solvent	43
16	The binding isotherm of STD-AF initial growth rates method	46
17	Determination of K_D with ITC experiment	49

LIST OF TABLES

TABLE Page

1 Quantitative DNP-NMR experiment with DMSO suppression showing different experimental conditions with D_2O solvent injection 17

2 Quantitative DNP-NMR experiment with DMSO suppression showing different experimental conditions with H_2O solvent injection 18

3 Quantitative DNP-NMR experiment showing fit parameters with D_2O solvent injection 33

4 Quantitative DNP-NMR experiment showing fit parameters with H_2O solvent injection 33

5 The fit parameters evaluated from STD-NMR 47

1. INTRODUCTION

Protein interactions with small molecules play a pivotal role in a wide variety of cellular processes. Enzyme-substrate, receptor-neurotransmitter and antibody-antigen interactions are a few examples of cellular processes involving interaction between proteins and small molecules. Drugs are designed and developed based on the knowledge of the substrate structure and the enzyme-substrate interaction. They are responsible for inhibiting the target enzyme or protein functions. An early and important step in drug design is identifying the binding interaction between protein and ligand by means of a fast screening of a wide variety of compound libraries. Such a task needs to be carried out efficiently. However, the affinities of promising lead compounds are typically low, requiring further chemical modification of the ligands. Targeted chemical modification requires the knowledge of detailed structural information of the protein binding pocket and the bound ligand.[1,2] The ligand binding component (ligand epitope) can be mapped through studies of the ligand resonances known as ligand-observed NMR.[1–6] Analysis of the protein resonances is required to obtain structural information of the protein and the protein binding pocket.[1,2] A number of solution NMR spectroscopic methods have been developed for investigation of the interactions between proteins and small molecules. Saturation Transfer Difference (STD) NMR has been widely used for studying binding between the proteins and the small molecules[7] and determining their binding association constant. Triple resonance protein-observed NMR spectroscopy has been a powerful method for structural determination of large proteins

(>17 kDa). Triple resonance experiments include correlations among three types spins (^{1}H, ^{13}C and ^{15}N), thereby requiring the use of the isotope labels ^{13}C and ^{15}N.[4,5]

In this study, DNP-NMR spectroscopy is applied for the investigation of the interaction of the protein with its hyperpolarized inhibitor ligand and characterization of the protein binding pocket by analysis of selectively enhanced protein NMR resonances. Trypsin and benzamidine are chosen as models for the protein and the ligand, since the binding of benzamidine to trypsin at the specific protein binding pocket is well-known.[8–15] The DNP-NMR technique is based on 1D time-resolved ^{1}H NMR studies of protein signal. DNP enables the analysis of enhanced trypsin signal due to the polarization transfer from hyperpolarized benzamidine. The polarization transfer rate determined from the DNP-NMR technique is compared to the cross-relaxation rate obtained from the conventional STD-NMR method. Analysis of selectively enhanced protein NMR resonances would in future studies be expected to eventually lead to identification of the amino acids residing in the protein binding pocket directly interacting with the hyperpolarized ligand.

1.1 Sensitivity of NMR

NMR spectroscopy has low sensitivity (signal to noise ratio) due to the small energy gaps between the nuclear spin states. Due to its low sensitivity, NMR techniques typically require the use of high concentration samples and long measurement time. A number of techniques have been developed to improve the sensitivity in NMR in the past several decades. One major improvement was the development of Fourier Transform NMR which enhanced the sensitivity by approximately 100 fold compared to continuous

wave NMR.[16] To put these into perspective, an increase in the magnetic field from 400MHz (9.4T) NMR to 900MHz (21.1T) NMR provides approximately 3-4 times improvement in sensitivity according to the proportional relationship between the signal to noise ratio (SNR) and a power of the magnetic field ($B_o^{3/2}$).[17] In the past, a number of hyperpolarization techniques, namely, chemically induced dynamic nuclear polarization (CIDNP)[18], optical pumping (OP)[19] and parahydrogen induced polarization (PHIP)[20,21] came into existence. In CIDNP, polarization is produced as a result of a thermal or photochemical reaction.[18] In OP, circularly polarized light is used to polarize the electron spin in alkali metal atoms, and polarization is then transferred from the electron spin of alkali metal atoms to the nuclear spin of noble gas.[19] In PHIP, parahydrogen is the source of polarization and transfers its polarization to unsaturated compounds with addition reaction or to small organic molecules which, along with parahydrogen, coordinate with the metal center.[20,21] However, the applicability of these hyperpolarization techniques is limited to certain molecules. Unlike these techniques, dynamic nuclear polarization (DNP) can be used to polarize almost any molecule. DNP enables signal enhancement from a few hundreds to ten thousands fold.[22]

1.2 Theoretical background on DNP

At typical magnetic fields, nuclear spins are approximately equally populating upper and lower energy levels, with a slight excess of population at the lower energy level at thermal equilibrium and, thus, there is little or no polarization (relative population difference between the lower and upper energy level) of the nuclear spins which leads to the low NMR signal intensity. A method of increasing the NMR signal

intensity by artificially creating a large population difference between two energy levels is called hyperpolarization of the nuclear spins. Hence, DNP technique artificially generates the polarization of the nuclear spins.

The general working principle of DNP is based on the transfer of polarization from electron spins to nuclear spins by microwave irradiation.[23] For a liquid state sample, the polarization transfer from the polarized electron to the nuclear spin occurs via the Overhauser effect.[23–25] The solid effect is a two-spin process of transferring the polarization from an electron spin to a nuclear spin for a sample with paramagnetic centers (such as free radicals).[24] The solid effect occurs in solid state samples. In our experiments, the sample containing the ligand, free radicals and glass-forming agents was frozen to a solid inside a DNP polarizer where the process of the polarization transfer from an electron spin to a nuclear spin occurs. Other mechanisms such as cross effect[26] or thermal mixing[26] are known to cause polarization transfer to a nuclear spin under certain conditions such as a high concentration of free radicals.[26]

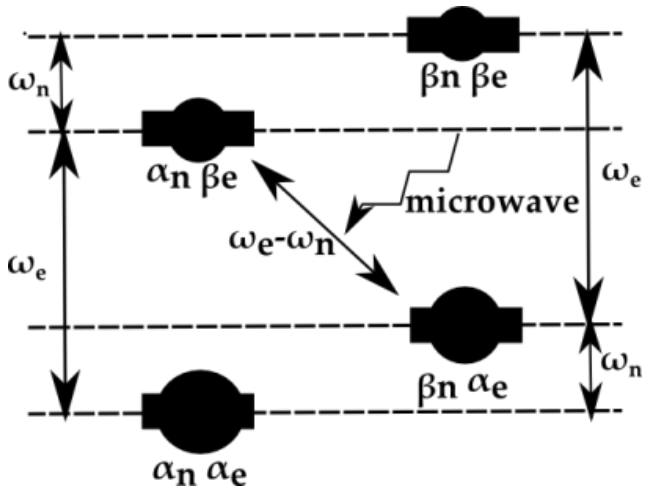

Figure 1. Scheme illustrating solid effect DNP. A nuclear spin (I=1/2) and an electron spin (S=1/2) dipole-coupled at thermal equilibrium to be perturbed using microwave irradiation at the transition frequency (ω_e-ω_n).[24] α represents the spin state at the lower energy level and β the spin state at the upper energy level. Subscripts e and n symbolize electron and nuclear spins, respectively. ω_n and ω_e represent the transition frequency for a nuclear spin and an electron spin, respectively. The size of the black circle represents the population. Note that figure is not drawn to scale.

Figure 1 shows an energy level diagram at the thermal equilibrium for a nuclear and electron spin coupled via the dipolar interaction. The transitions with higher energy are due to the electron spin, and those with lower energy due to the nuclear spin. The size of gray spheres, which is not drawn to scale, represents the populations. Excitation of the $\alpha_n\beta_e$ spin state to the $\beta_n\alpha_e$ spin state with the microwave together with the relaxation of the $\alpha_n\beta_e$ spin state to the $\alpha_n\alpha_e$ spin state results in the larger population difference between the nuclear spin states ($\beta_n\alpha_e$ and $\alpha_n\alpha_e$).

In the dissolution DNP method, the sample containing paramagnetic centers and glass-forming solvent is prepared at room temperature. The glass-forming solvent (e.g water/ethanol, water/glycerol or water/DMSO) is used to ensure the function of a homogeneous solid so that diffusion of polarization can take place effectively.[25] The polarization is introduced to the sample after it is frozen to a solid state at approximately 1.4 K. Owing to their high gyromagnetic ratio (γ_e/γ_H~660), electron spins are almost completely polarized at 1.4 K and at a magnetic field of 3.34 T. The transition (ω_e-ω_n) is then irradiated with microwaves to hyperpolarize the nuclear spins ($\alpha_n\alpha_e$ and $\beta_n\alpha_e$) (Figure 1).

1.3 DNP-NMR methods for study of chemical and biological systems

Recently, dynamic nuclear polarization (DNP)-NMR techniques have emerged as a tool for time-resolved studies of interactions between different molecules.[27–29] Polarization of molecules with DNP results in significant enhancement of the signals, thereby enabling real-time analysis of the signal of polarized molecules and of the molecules interacting with polarized molecules. A number of studies showed that time-resolved NMR spectra can be obtained with rapid injection of polarized molecules from DNP for studying transient processes and elucidating reaction mechanism involving short-lived reaction intermediates.[30] Although the dissolution DNP-NMR method has primarily been employed for polarization of small molecules, a recent study showed that time-resolved high-resolution NMR spectra of polypeptides can be acquired with the polarization of polypeptides using DNP.[31] In the work described here, a ligand (small molecule) was hyperpolarized in DNP, and rapidly injected into the NMR tube

preloaded with the protein sample inside the NMR spectrometer. The time-dependent process of signal transfer to protein was monitored by the NMR instrument. The time-resolved signal buildup and decay of the ligand and the protein was fitted into the model equations describing the polarization signal transfer process.

1.4 Nuclear Overhauser Effect (NOE)

NOE is the change in the intensity of a spin (I) when the population of another spin (S) coupled to spins (I) is perturbed.

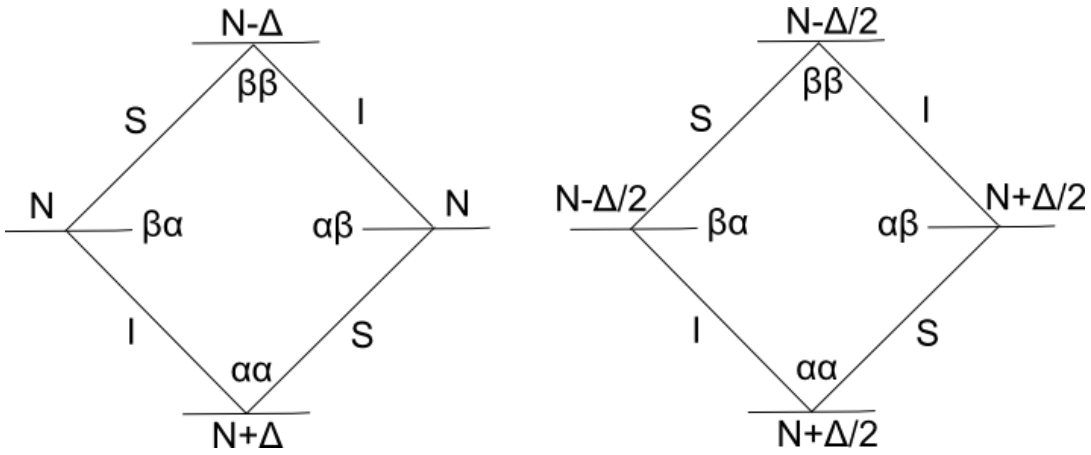

Figure 2. Energy level diagram showing spin populations in a two spin system. The diagram on the left shows the spin states of the dipolar-coupled spin system (S and I) and their population at Boltzmann equilibrium. The diagram on the right shows the state of the same spin system as a result of the saturation on spin S before NOE occurs.

NOE can be mathematically described as $\frac{I - I_o}{I_o}$ where I is the signal intensity of spin I upon perturbation of spin S and I_o is the signal intensity of spin I in the absence of

perturbation. The NOE value can be obtained by analysis of the change in intensity of spin (I) that couples with the spin (S) via the dipolar interaction. Dipolar interaction is the disturbance of the magnetic field of one nuclear spin by the magnetic field of the other spin.

The diagram on the left of figure 2 shows the equilibrium population of a spin system involving spin S and spin I, which are in close spatial proximity and coupled via the dipolar interaction. The diagram on the right illustrates the changes in the population of different spin states upon saturation of the spin. These two transitions denoted by I or S represent the spin (I) transition and the spin (S) transition. N represents the size of the population of a particular spin state. There are four different possible spin states denoted by αα, αβ, βα and ββ. Different spin states occupy different energy levels. +Δ symbol represents the population surplus and -Δ represents the population deficit. When spin (S) is saturated with a selective irradiation, the populations across the (S) transitions become equalized. The signal intensity of spin (S) decreases or vanishes after saturation.

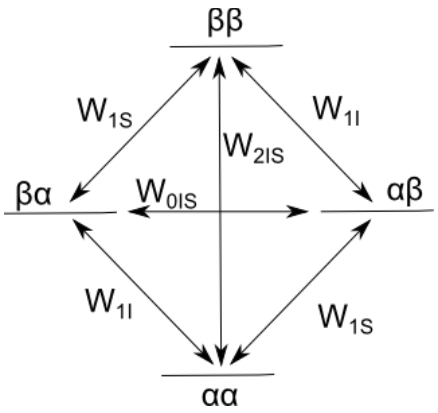

Figure 3. Relaxation pathways in an irradiated two spins system.

There are six relaxation pathways for the coupled sp

in system. W denoted with subscript 1 represent T_1 relaxation pathways, whereas W donated with subscript IS represents the cross-relaxation pathways. Double quantum transition W_{2IS} and zero quantum transition W_{0IS} are cross-relaxation pathways mainly responsible for NOE. The difference between the two is defined as the cross-relaxation rate (σ). Whether the NOE value is positive or negative depends on whether W_{2IS} or W_{0IS} is dominant. When the double quantum (W_{2IS}) relaxation pathway is dominant (the NOE value is positive), there will be a larger population difference for spin (I) than there is at equilibrium. As a result, a larger intensity of spin (I) can be observed. Conversely, when zero quantum (W_{0IS}) relaxation is dominant, the population difference becomes smaller and the signal intensity of spin (*I*) decreases accordingly. For a large molecule such as a protein, W_{0IS} (zero quantum transition) is more probable and, thus, negative NOE can be expected.

The steady-state NOE equation ($\frac{I-I_0}{I_0}$) described above is derived from the Solomon Equations. Solomon equations describe the evolution of spins towards the equilibrium after the spins are perturbed.[32]

$$\frac{d\left\langle I_z - I_0 \right\rangle}{dt} = -R_{IS}\left\langle I_z - I_0 \right\rangle - \sigma_{IS}\left\langle S_z - S_0 \right\rangle \qquad \text{(I.1)}$$

where $R_{IS} = W_{0IS} + 2W_{1I} + W_{2IS} = \frac{\hbar^2\gamma_H^4}{4r_{IS}^6}\{J_{IS}(0) + 3J_{IS}(\omega_H) + 6J_{IS}(2\omega_H)\}$ and

$$\sigma_{IS} = W_{2IS} - W_{0IS} = \frac{\hbar^2\gamma_H^4}{4r_{IS}^6}\{6J_{IS}(2\omega_H) - J_{IS}(0)\}$$

I_z and S_z represent the magnitude of the z component of magnetization (z-magnetization) of the coupled spins I and S respectively.[33] Subscript (0) on the spin labels denotes the Boltzmann equilibrium state. Note that perturbation is applied on the spin S. Under the static magnetic field, the magnetic dipole moment of individual spins is aligned along the z-direction at the Boltzmann equilibrium. The total magnetic dipole moment created by an ensemble of the spins is defined as the z-magnetization.

The magnitude of z-magnetization of spins at the steady state is dictated by the longitudinal relaxation rate (R_{IS}) and the cross-relaxation rate (σ_{IS}). R_{IS} and σ_{IS} are dependent upon the spectral density *J(ω)* which describes how much power the local fluctuating magnetic field caused by random tumbling molecules can supply to induce a transition of a particular frequency ω. In other words, it is a measure of the probability of the transition at a particular frequency ω. The spectral density *J* at a particular frequency ω is expressed by[34–36]:

$$J(\omega) = \frac{2\tau_c}{(1+\omega^2\tau_c^2)} \tag{I.2}$$

where $\tau_c = \frac{4\pi\eta r^3}{3kT}$

Spectral density J is dependent on the correlation time τ_c, which is a function of viscosity (η), the molecular mass (*r*) and the temperature (*T*).

Solving the steady state Solomon equation (i.e. $\frac{d\langle I_z - I_0\rangle}{dt} = 0$) upon a complete saturation of the perturbed spin (S) (i.e. $\langle S_z\rangle = 0$) yields [37,38]

$$\frac{I_z - I_0}{I_0} = \frac{\sigma_{IS}}{R_{IS}} \frac{S_0}{I_0} \tag{I.3}$$

Since the proton spin population difference under the Boltzmann equilibrium condition is proportional to the gyromagnetic ratio of the proton, the ratio of the magnetization of spin S to that of spin I can be given by[37,38]:

$$\frac{S_0}{I_0} = \frac{\gamma_{H,S}}{\gamma_{H,I}} = 1 \tag{I.4}$$

Therefore, it follows that the fraction of the change in the signal intensity of spin I interacting with perturbed spin S can be expressed as[37,38]:

$$\frac{I_z - I_0}{I_0} = \frac{\sigma_{IS}}{R_{IS}} \tag{I.5}$$

This equation shows that the observed NOE signal intensity of spin I is the result of cross-relaxation.[39]

It can be noted in the equation (I.5) that the cross-relaxation rate (σ) shows dependence on the inverse sixth power of the distance between the two coupled spins. Hence, the proximity of the two coupled spins can be quantified from the measurement of σ value.

Saturation Transfer Difference NMR (STD-NMR) which is described in detail in the next section is based on the NOE effect between the saturated spin of the protein and the spin of the ligand.

1.5 Saturation Transfer Difference NMR (STD-NMR)

STD-NMR spectroscopy has been widely used as a ligand-based NMR technique for (i) detection of the binding interaction between the protein and the ligand, (ii)

determination of a dissociation constant (K_D) [40] and (iii) mapping of the ligand epitope (determination of orientation and structural components of ligand at the site of binding).[41–46] STD exploits the steady-state Nuclear Overhauser Effect (NOE) which is the transfer of magnetization (M_z) (to be specific "saturation" signal in STD-NMR) from the perturbed spin (protein proton spin) to another spin (ligand proton spin) in close proximity through the dipolar interaction at the steady state.

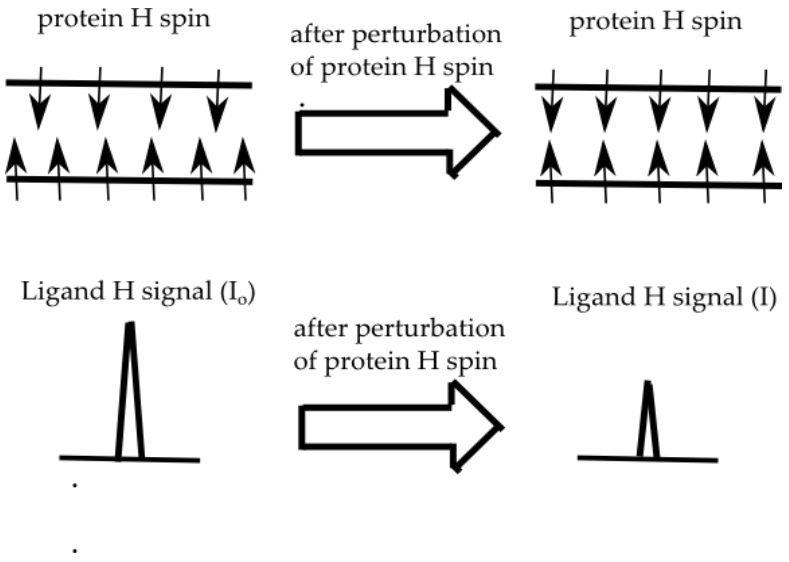

Figure 4. Illustration of the STD-NMR experiment. The top figure shows the perturbation (saturation) of the protein spin. The bottom figure shows the change in the signal intensity of the ligand as a result of its interaction with the saturated protein.

In the STD-NMR method, the signal intensities of the spins are observed when the populations of the spins are at the steady-state. Experimentally, the protein proton spin is selectively perturbed (saturated) with irradiation of the so-called the on-resonance

frequency. The signal intensity of the ligand (I) observed at the on-resonance condition is compared with the signal intensity of the ligand (I_o) observed under the off-resonance condition from a reference spectrum. The difference between on-resonance and off-resonance spectrum (I_o-I) provides qualitative information about the extent of the binding between the protein and the ligand. The binding strength can be quantitatively evaluated from the STD-NMR experiment. In the STD-NMR protein-ligand titration experiment, fitting the mathematical model equation of *STD-AF* with the STD-NMR experimental data generates the dissociation constant (K_D), which is a measure of the binding affinities between ligand and protein.

In addition, information on the proximity of different proton spins of the ligand to the protein can also be deduced from the variation of the STD signals with the elimination of the effect due to variation in relaxation rates of different proton spins. Stronger STD signals are interpreted as a shorter distance between ligand and receptor protons. This interpretation arises from the distance dependence of the NOE signal transfer process. Hence, mapping the ligand epitope at the binding site (identifying which parts of the ligand are involved in the binding interface) can be accomplished with the STD-NMR method.[4,47–49]

STD amplification factor (*STD-AF*) can be mathematically defined as [48,50]:

$$STD-AF = \frac{I_0 - I_{sat}}{I_0}\frac{[\text{Ligand}]}{[\text{Protein}]} \tag{I.6}$$

The STD method has its limitations in terms of application. The STD method is not suitable for strongly binding ligands with K_D approximately <1 nM since the STD ligand

signal intensity is reduced when strongly binding ligands are used. A long residence time of the strong binder ligands at the protein binding site results in the fast relaxation of the ligand bound to the protein and, thus, loss of the signal. [3,51] On the other hand, the population of ligand-receptor complex decreases for weakly binding ligands having $K_D > L_T$, (L_T-total ligand concentration), resulting in the attenuation and disappearance of the STD effect. The K_D range within which the STD-NMR method can be applied is approximately $10^{-3} > K_D > 10^{-8}$ M. [3,51]

There are several advantages to using the STD-NMR method. First, it only requires a low concentration of protein (~1 μM).[52,53] The population of the saturated ligand builds up during the period of the sustained irradiation. Since the ligand exchange typically takes place rapidly, a small amount of protein can generate an amplified amount of saturated ligand.[49] Second, STD-NMR is an ideal method to use with large protein masses, (>30000 Da). Owing to its large rotational correlation time τ_c, large protein enables an efficient signal propagation within itself via spin-diffusion and, thus, enhances signal transfer to the ligand. Another advantage is that signal contribution from the free-state does not need to be corrected for the observed signal intensity, since the observed signal is a result of bound ligands or ligands that have already bound to the receptor. That, thus, simplifies the data interpretation and reduction.[3]

2. EXPERIMENTAL METHODS

2.1 DNP-NMR experimental setup and method

18 μL of 510 mM benzamidine and 2 μL of 150 mM TEMPOL free-radical in 80%v (99.9% [D_6] DMSO) and 20%v D_2O underwent hyperpolarization in a HyperSense system (Oxford instruments, Abingdon, U.K.) by irradiating a 100 mW power at 94.005 GHz frequency for 30 min, at a temperature 1.4 K. Hyperpolarized samples were dissolved by a stream of heated 50 mM potassium phosphate buffer solvent at pH 7.0 and automatically loaded into an injection loop. The initial 450 μL of sample solution in the loop representing an estimated 40% of benzamidine (estimated by HPLC) was injected into a 5 mm NMR tube containing 25 μL of 2.4 mM trypsin dissolved in 50 mM potassium phosphate preinstalled in a 400MHz NMR spectrometer (Bruker Biospin, Billerica, MA).[54] The reaction time assigned for the first NMR spectrum from the start of the interaction between trypsin and benzamidine was estimated to be the sum of half of the injection time (0.215 s), the stabilization time (0.1 s) and the time for all the initial pulse sequence events (0.255 s) prior to the beginning of the FID acquisition. The estimated final concentration after dissolution in the NMR tube was 118 μM for trypsin (concentration estimated using UV) and 7.7 mM for benzamidine (concentration estimated using HPLC).

Upon injection of the hyperpolarized benzamidine into the trypsin sample, multiple spectra of the sample containing a mixture of tryspin and benzamidine were taken with a series of fixed small flip angle (15^o) excitations. The correction factor $e^{-\lambda t}$ (where λ was calculated to be -0.18 using the small flip angle)[54] was applied to

compensate for the decrease in the size of the z-magnetization for the same small flip angle with each subsequent scan. After a small 15^{o} flip angle pulse, 1638 data points were collected over 0.128 s. The time interval between each scan was 0.2 s.[54]

The final concentrations of trypsin in the NMR tube at the end of the DNP experiment were determined based on the total volume (475 μL) of sample in the NMR tube obtained after injection of hyperpolarized benzamidine solutions on the initial 25 μM of trypsin stock solution preloaded in the NMR tube. The concentration of the trypsin stock solution was measured with UV spectrophotometry, using the extinction coefficient 37650 $M^{-1}cm^{-1}$.[55]

The concentration of benzamidine in the NMR sample with trypsin in the DNP-NMR experiment was determined based on the concentration of pure benzamidine solution in the NMR tube in the control DNP-NMR experiment, since the same experimental conditions including injection parameters were set in both experiments. The concentration of benzamidine was determined with HPLC.

In optimizing the dissolution DNP-injection system, the following conditions/issues have to be considered. A fast injection system to transport the polarized sample to the NMR tube is essential to minimize the loss of polarization signal. A long enough waiting time to allow for stabilization of the sample after injection is also required to obtain NMR resonances with a narrow line-width. Injection by application of high pressure can cause bubble formation in the NMR tube which can give rise to issues such as line-width broadening and spectra distortion. On the other hand, injection with low pressure can lead to poor mixing between polarized sample and

preloaded sample. Therefore, the balance of all of these conditions has to be achieved for acquiring quality spectra.

Table 1. Quantitative DNP-NMR experiment with DMSO suppression showing different experimental conditions with D_2O solvent injection

DNP Experiment #	stabilization time (ms)	half injection time (ms)	pulse sequence before acquisition (ms)	time for 1st data point (ms)	Time between each scan (ms)	total volume in NMR tube (µL)	initial conc of trypsin /Protein Stock (mM)	[P],conc of trypsin in NMR tube (µM)	initial conc of benzamidine (mM)	[L], conc of benzamidne in NMR tube (µM)	*pb* (fraction of bound ligand),K_D=80 µM
3121	0.1	0.255	0.127	0.482	0.2	475	2.24	118.0028	500	6100	0.019
3101	0.1	0.255	0.127	0.482	0.2	475	2.24	118.0028	500	6100	0.019
3131	0	0.255	0.127	0.382	0.2	475	2.24	118.0028	500	6100	0.019
3241	0	0.255	0.127	0.382	0.2	475	2.55	134.447	500	6900	0.019
3261	0	0.255	0.127	0.382	0.2	475	2.55	134.447	500	6900	0.019
2651	0.1	0.205	0.127	0.432	0.2	475	2.5	131.5789	500	10557	0.0124

***** Time for the 1st data point=stabilization time + ½ injection time + pulse seq. time prior to acquisition

*pb (fraction of bound ligand) is needed to evaluate the fit parameters in DNP model shown in section 3.4. pb was calculated using the formula[56]

$$p_b = \frac{[P]_t + [L]_t + K_D - \sqrt{([P]_t + [L]_t + K_D)^2 - (4[P]_t[L]_t)}}{2[L]_t}$$

Table 2. Quantitative DNP-NMR experiment with DMSO suppression showing different experimental conditions with H_2O solvent injection

DNP Experiment #	stabilization time (ms)	half injection time (ms)	pulse sequence before acquisition (ms)	time for 1st data point (ms)	Time between each scan (ms)	total volume in NMR tube (µL)	initial conc of trypsin /Protein Stock (mM)	[P],conc of trypsin in NMR tube (µM)	initial conc of benzamidine (mM)	[L], conc of benzamidne in NMR tube (µM)	pb (fraction of bound ligand),K_D=80 µM
3331	0	0.255	0.127	0.482	0.2	475	2.55	134.447	500	7800	0.017
3341	0	0.255	0.127	0.482	0.2	475	2.55	134.447	500	7800	0.017
3361	0	0.255	0.127	0.382	0.2	475	2.55	134.447	500	7800	0.017
3321	0	0.255	0.127	0.382	0.2	475	2.55	134.447	500	7800	0.017

2.2 DNP-NMR pulse program

The DNP-NMR experiments were measured using small flip angle (α) pulses. Different time steps involved in the experiment were shown in figure 5. The transfer of polarized sample from the polarizer was carried out using the home-built sample injector for a transfer time (t_t) shown in figure 5. Sample mixing occurred at the half of the injection time (t_i). A waiting (stabilization) time (t_s).

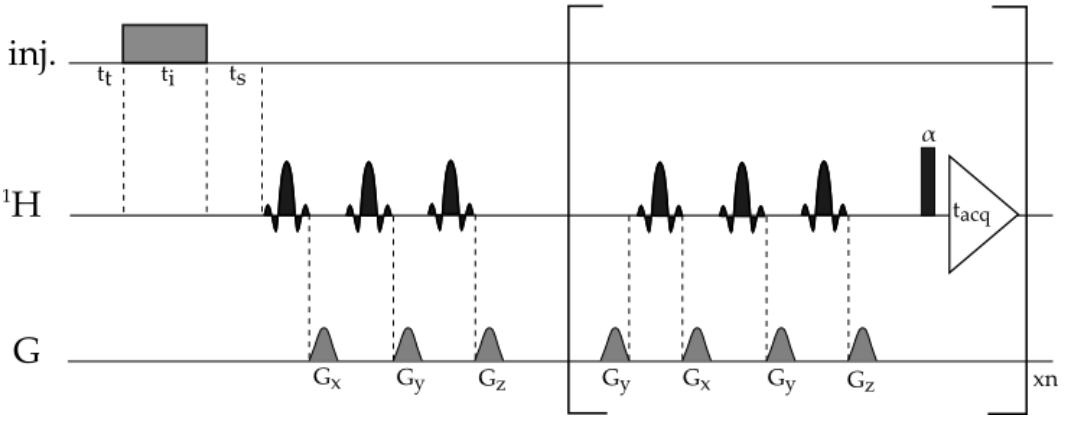

Figure 5. DNP-NMR pulse sequence[29]

Solvent suppression was achieved by selective excitation of water and dimethyl sulfoxide (DMSO) proton residue in D_6-DMSO dissolution solvent. The water solvent and DMSO solvent were selectively suppressed, since the resonance frequency difference between water and the nearest resonance of interest was approximately 1100 Hz. The first spectrum was acquired using six EBURP2 shaped π/2 pulses to suppress water resonance at 4.7 ppm and DMSO at 2.7 ppm dephased by randomized pulsed field gradients G_x, G_y or G_z.[30] Later scans were preceded by three EBURP2 shaped π/2 pulses,

each of which was dephased by randomized pulse field gradients G_x, G_y or G_z.

2.3 DNP-NMR spectra and data processing

An exponential window function with a line broadening of 10 Hz was applied before Fourier transformation using the TOPSPIN 3.1 program (Bruker Biospin, Billerica, MA) for NMR spectra from DNP experiments.[54]

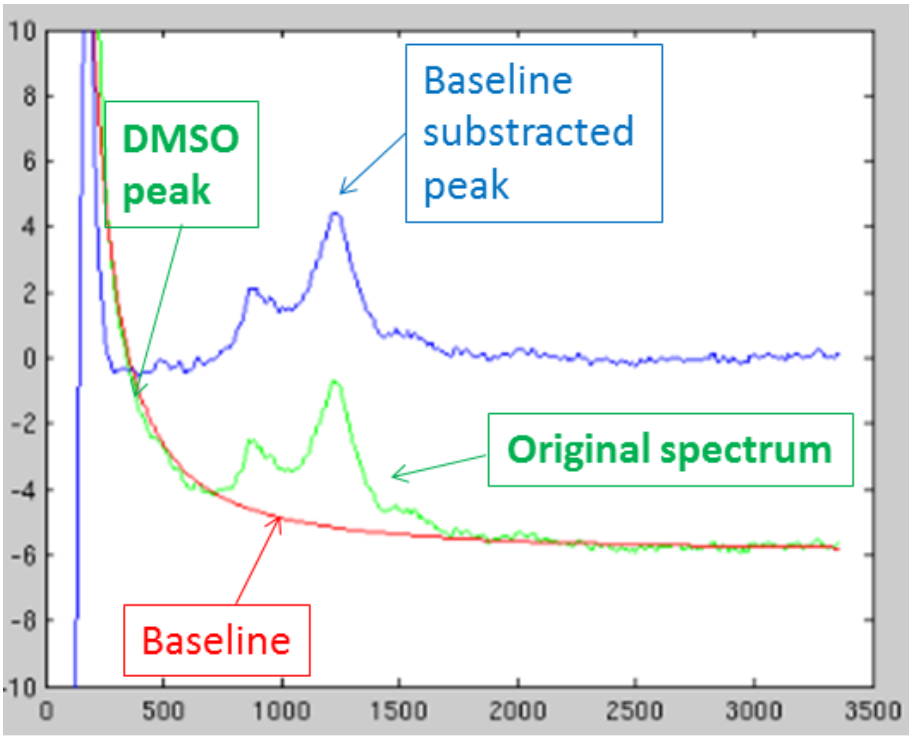

Figure 6. Mathematically defined baseline for the peak. The mathematical function (red color) was used to define the baseline subtracted from the original spectrum. The image shows the display as seen in the Matlab software interface during data processing.

The DNP spectra from initial experiments (not shown here) showed that the neighboring water and the proton DMSO solvent peaks overlapped with the selectively

enhanced trypsin peak at 1.2 ppm. Therefore, the effect of neighboring peaks has to be removed prior to integration of the selectively enhanced trypsin signals to obtain an accurate signal intensity. Integration of the selectively enhanced peak of trypsin and benzamidine peak was carried out in MATLAB (The MathWorks, Natick, MA). The functions $(a+b/(x-x_o))$ and $(a+b*(x-x_o))$ were used to define the baseline for the selectively enhanced signal of trypsin and hyperpolarized benzamidine signal respectively to remove the baseline effect of the neighboring peaks.

However, the spectra from the newer experiments were free from the large neighboring proton DMSO residue peaks. A straight- line function baseline was manually defined for both trypsin and benzamidine peak in Topspin software. A typical range of the straight line baseline for trypsin was approximately between 3 ppm to -1 ppm. The model equation fitting (shown in section 3.4) was performed in Mathematica (Wolfram Research, Champaign, IL).

2.4 STD-NMR pulse program

For the STD experiments, a pseudo 2D pulse program (stddiffesgp.3) installed on the Bruker software was used to acquire the on and off resonance spectra. On-resonance irradiation was set to 1.2 ppm and off-resonance irradiation was set to 14 ppm. A train of 90^o Gaussian-shaped saturation pulses was applied for a duration of 100 ms. 180^o shaped pulse using excitation sculpting with gradients for the duration of 2 ms was applied for the water solvent suppression and suppression of residual DMSO in D_6-DMSO. In different experiments, a total number of scans ranging from 96 to 192 was acquired. A larger number of scans was applied for samples with a low concentration of ligand.

3. RESULTS AND DISCUSSION

3.1 Selectively enhanced NMR resonances in DNP-NMR

Trypsin and benzamidine were chosen as models for protein and ligand since the binding of benzamidine to trypsin at the specific binding site has already been known and their dissociation constants have been reported in the literatures.[8–11] Benzamidine was hyperpolarized on its proton nuclei in the solid state by DNP, dissolved and transferred to a nonpolarized solution of trypsin in the NMR spectrometer. Hyperpolarized signal was transferred from benzamidine to trypsin when benzamidine binds to trypsin.

Figure 7 shows that the protein NMR signals were selectively enhanced through binding of the hyperpolarized ligand. in DNP-NMR. Polarization signal was transferred from benzamidine to trypsin when benzamidine binds to trypsin.

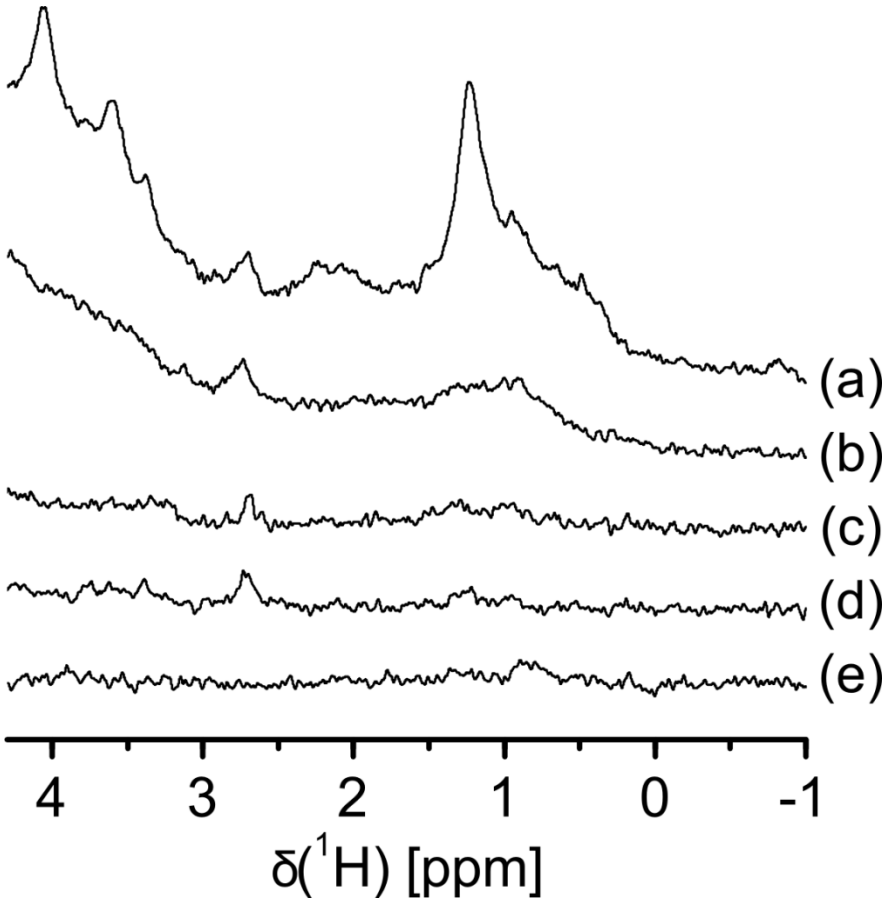

Figure 7. 1D stacked proton NMR spectra in the DNP-NMR experiment. (a) hyperpolarized benzamidine with trypsin, (b) hyperpolarized benzyl alcohol with trypsin, (c) hyperpolarized [D_6]DMSO/D_2O with trypsin, (d) hyperpolarized [D_6]DMSO/D_2O with no trypsin and, (e) non-polarized benzamidine with trypsin by injection of benzamidine in D_6-DMSO/D_2O without polarization into trypsin loaded NMR tube [mock injection DNP experiment]

The selective signal enhancement of trypsin with hyperpolarized benzamidine was pronounced at 1.2 ppm and 4 ppm as shown in figure 7 (a). Other less pronounced enhanced signals were observed approximately at 3.6 ppm, 3.3 ppm, 2.2 ppm and -0.8

ppm. With hyperpolarized benzyl alcohol, there is no enhancement of the trypsin signal in figure 7 (b). An enhancement due to non-specific interaction between protein and the solvent was also found to be negligible in figure 7 (c). We used the control experiment using the polarized solvent (D_6-DMSO/D_2O) only without trypsin in figure 7 (d) to show that the small signal at 2.7 ppm shown in figure 7 (b) and (c) is not due to the non-specific interaction between the protein and the ligand but to the proton residue of D_6-DMSO solvent. In the experiment with no polarization of benzamidine with trypsin shown in figure 7 (e), no enhancement of trypsin signal was observed.

3.2 Comparison of the DNP-NMR and STD-NMR spectrum

The three spectra in figure 8 represent the spectra of trypsin from different experiments.

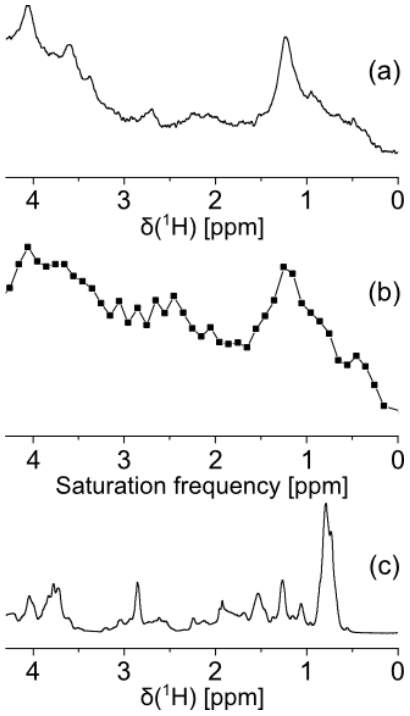

Figure 8. Comparison of trypsin spectrum from different experiments. (a) shows enhanced trypsin proton NMR signal with polarization of benzamidine in the DNP-NMR experiment as in figure 7. (b) shows the plot of the fractional change in the ligand signal intensity versus trypsin saturation frequency using benzamidine (400 μM) and trypsin (80 μM) in the STD-NMR experiment with the saturation time of 20 s. (c) shows 1D proton conventional/non-hyperpolarized NMR spectrum of trypsin.

In parallel to the DNP-NMR experiment shown in figure 7 and figure 8 (a), we conducted the STD experiment in which trypsin was selectively saturated at a series of on-resonance frequencies within a wide range of proton frequency of interest shown in figure 8 (b). An array of on-resonance frequencies were chosen to ensure that saturation at a continuous spectrum of frequencies is achieved. The plot of the fractional change in

the ligand signal intensity ($(I_{0L}-I_L)/I_{0L}$) or fractional STD enhancement versus the on-resonance frequency for the saturation is shown in figure 8 (a). In general, the shorter the saturation time that is employed, the weaker the STD signal that is obtained. Therefore, we can expect that the STD signal with a longer saturation time would be associated with less error. It can be noted that the DNP-NMR spectrum of trypsin in figure 8 (a) is different from the conventional 1D NMR spectrum of trypsin in figure 8 (c). That suggests the signal enhancement is of the local protein binding pocket to which hyperpolarized benzamidine binds, rather than the signal enhancement of the entire protein region. The maximum signal occurs at the two frequencies 1.2 ppm and 4.0 ppm.

The spectrum in figure 8 (a) was calibrated as follows. Immediately after the polarization experiment (the acquisition of the DNP-NMR spectrum), a non-hyperpolarized spectrum was taken. DMSO proton residual solvent peak in the non-hyperpolarized spectrum is calibrated against DMSO proton residual peak of the similar sample. In figure 8 (b) and (c), chemical shifts of the sample were calibrated against those of (4,4-dmethyl-4-silapentane-1-sulfonic acid) DSS present in similar standard samples. The benzamidine peaks in the sample and standard sample were then matched and set to the same frequency.

The comparison of the selectively enhanced protein spectra (a single scan) obtained from DNP-NMR experiment with the STD ligand spectra constructed from a set of STD-NMR measurements across the wide range of protein frequencies suggests that the two experiments are symmetrical. The symmetry of the two experiments is not unexpected since, in DNP-NMR, the polarization signal transfers from the

hyperpolarized ligand to the protein binding sites, whereas the saturation signal transfers from the protein binding sites to the ligand in STD-NMR.

There are significant advantages of the DNP-NMR method over the STD-NMR method. The comparison of Figure 8 (a) and (b) shows that the signal intensity profile obtained with the DNP-NMR method provides a much better resolution than the profile obtained from the STD-NMR experiment. In addition, the experimental and signal-processing time in the DNP-NMR experiment is on the time scale of a few seconds to several seconds after a hyperpolarization period of 30 min, whereas the experimental time and signal-processing time for the STD-NMR experiment takes from several days to a few weeks.

3.3 Analysis of different peaks in STD-NMR

The STD signal $((I_o - I)/I_o)$ at different protein saturation frequencies was acquired using different saturation times shown in figure 9. The STD signal acquired with shorter saturation times has a much lower signal to noise ratio and is associated with more errors than the signal obtained using a longer saturation time.

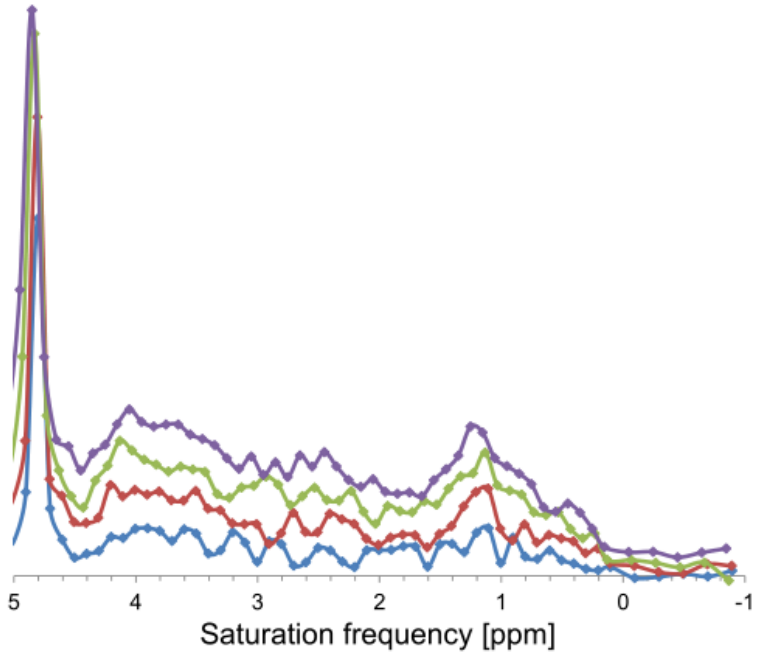

Figure 9. STD signal at different saturation frequencies. Spectra stacked for different saturation times: 20 s, 3 s, 2 s and 1s respectively from top to bottom, using benzamidine (400 μM) and trypsin (80 μM)

The saturation signal is a function of both the cross-relaxation rate (σ) and the auto-relaxation rate (ρ) of spins. Different spins (ligand spins in the STD experiment) that receive the signal from the perturbed spins (saturated protein spins in the STD experiment) can relax back to equilibrium at different auto-relaxation rates. Similarly, different spins can receive signal from the perturbed spins and their cross-relaxation rates (σ) can vary with their proximity to the perturbed spins. Theoretically, different spins with a different resonance frequency can reach the steady-state at different saturation times due to different environments they are in (i.e. they can have different σ

and ρ values). A rational choice of a proper saturation time would be to find the saturation time when spins reach the steady-state.

The frequency of the maximum peaks slightly changes when compared at different saturation times shown in the figure 9 of section 3.3, perhaps, due to the errors arising from the signal intensity measurement at shorter saturation times. Therefore, the most rational choice of the proper saturation time would be the longest saturation time (20 s in this experiment) that allows for the STD signal with the least amount of errors. An alternative explanation for the slight unidirectional shift in the frequency of the maximum peaks with the progression of saturation time is that different spins with very similar frequencies could have different saturation buildup times and, thus, display maximum saturation signal at different saturation times.

3.4 Signal buildup in the time-resolved DNP-NMR spectra

With the DNP experiments, the polarization signal decay of the ligand and that of protein polarized due to cross-relaxation with the hyperpolarized ligand during the transient period was studied. The transient period lasted for several seconds until the polarization reaches the Boltzmann equilibrium. The equation for the evolution of the hyperpolarized signal (I_z) towards the Boltzmann equilibrium is shown in the literature. Time-dependent evolution of the hyperpolarized signal (I_z) towards the Boltzmann equilibrium is given in the literature.[29]

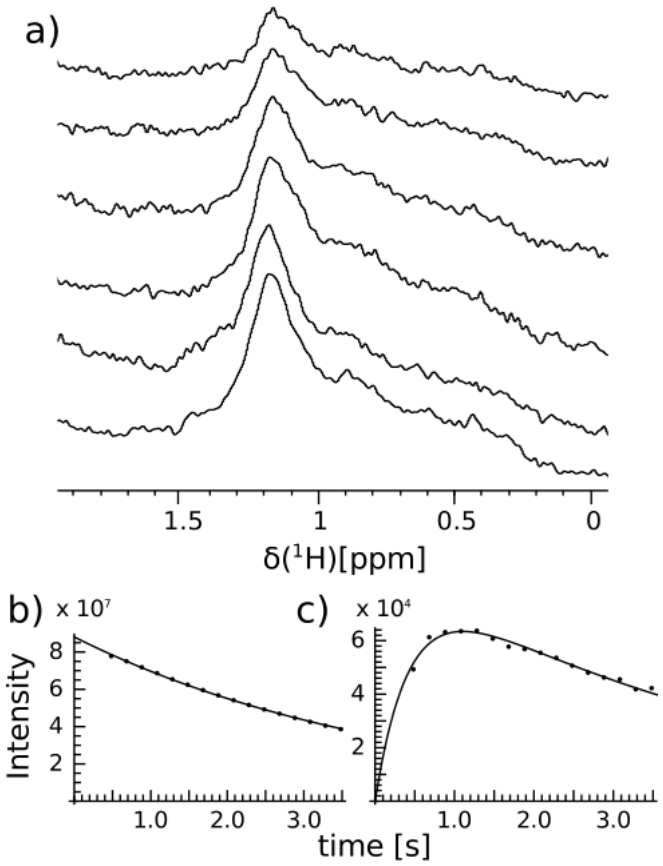

Figure 10. Polarization signal of trypsin and benzamidine in DNP experiment. (a) shows the expanded picture of a series of 1D proton NMR spectra showing protein transferred signal at 1.2 ppm; the integral of ligand in (b) and the integral of protein from 1 ppm to 1.3 ppm in (c) as a function of time. Integrals of ligand and protein were fitted with model equations. The water solvent resonance was selectively suppressed by EBURP2 shaped $\pi/2$ pulses of 20 ms duration.

The protein and the ligand were assumed as two coupled spins (one spin for the protein (P) and one spin for the ligand (L)) in derivation of the model equations representing the NMR signal intensities of the protein and the ligand.

The model equations for the ligand signal (s_L) and the protein signal (s_P) are given by[57]

$$s_L(t) = s_{LH} e^{-r_L t} \tag{III.1}$$

$$s_P(t) = \frac{(e^{-r_L t} - e^{-r_P t})\sigma^* s_{LH}}{r_L - r_P} = \frac{(e^{-r_L t} - e^{-r_P t})\sigma_{DNP} p_b s_{LH}}{r_L - r_P} \tag{III.2}$$

$r_L = p_f \rho_{Lf} + p_b \rho_{LP}$ and $r_P = p \rho_P + p_1 \rho_{PL}$, are averages of auto-relaxation rates weighed with concentration fractions, whereas $\sigma^* = \sigma_{DNP} p_b$ is the cross-relaxation rate weighed with concentration fraction (p_b) which represents the fraction of bound form of the ligand, and p and p_1 represent the fractions of free and and bound form of the protein. σ stands for the cross-relaxation rate between ligand proton and protein proton. The parameters ρ labeled with the subscripts (LP) and (PL) represent the auto-relaxation rates of the ligand when bound to the protein and of the protein when bound to ligand respectively. It can be noted that the protein signal is proportional to the cross-relaxation rate (σ), the fraction of the bound ligand (p_b) and the initial signal intensity of the ligand (s_{LH}).

Multiple spectra were taken with a series of fixed small flip angle (15^o) excitations.[54] Before fitting was performed, the signal intensity values were multiplied with the correcting term ($e^{-\lambda t}$) to compensate for the signal loss with each subsequent scan from applying a fixed small flip angle. The value for the parameter λ (-0.18) was calculated from the small flip angle and the time interval between each scan (0.2 s).[54] Equations (III.1) and (III.2) were used to fit the experimental data from DNP.

Figure 10 (a) shows a series of the selectively enhanced protein signal at approximately 1.2 ppm from multiple scans taken during a transient period of a few seconds. Since the interaction between hyperpolarized ligand and protein occurs prior to the acquisition of the first NMR spectrum, nonzero enhanced signal intensity of protein was observed in the first spectrum in figure 10 (b). As time progresses, the protein signal intensity increases initially as the protein accumulates polarization signal from hyperpolarized ligand and reaches the maximum signal approximately at 1 s and starts to decrease until the protein proton spins reach the Boltzmann equilibrium. For hyperpolarized ligand, the polarization signal intensity decreases exponentially as predicted by the model equations.

The initial signal intensity of the ligand (s_{LH}) and the apparent relaxation rate of the ligand (r_L) were first determined by fitting the data for the signal intensity of the ligand to the equation III.1 (in the bottom left trace of figure 10). These two parameters were set to known values in the equation (III.2) which is used to fit the data for the signal intensity of protein. The equation for the protein signal intensity generates the relaxation rate of protein (r_P) and cross-relaxation rate (σ_{DNP}). Fraction of bound ligand (p_b) shown in section 2.1, Table 1 and 2 was calculated using the K_D value obtained from STD experiment in section 3.9.

Table 3. Quantitative DNP-NMR experiment showing fit parameters with D_2O solvent injection

Experiment #	s_{LH} (A.U.)	$r_L(s^{-1})$	$r_P(s^{-1})$	σ_{DNP} (s^{-1})
3121	88100000	0.23	2.34	-0.114
3101	88100000	0.23	3.47	-0.098
3131	115000000	0.17	2.43	-0.079
3241	91700000	0.18	2.44	-0.094
3261	879000000	0.23	2.36	-0.086
2651	144000000	0.18	1.44	-0.112
Average		0.203333333	2.413333	-0.097
Standard Deviation		0.029439203	0.643915	0.0139

Table 4. Quantitative DNP-NMR experiment showing fit parameters with H_2O solvent injection

Experiment #	s_{LH} (A.U.)	$r_L(s^{-1})$	$r_P(s^{-1})$	σ_{DNP} (s^{-1})
3331	93196600	0.307	2.503	-0.061
3341	63980740	0.339	2.727	-0.090
3361	93708601	0.285	2.795	-0.067
3321	72718116	0.266	3.186	-0.075
Average		0.29925	2.80275	-0.073
Standard Deviation		0.031352	0.284329	0.013

The integral of the resonance corresponding to the phenyl group of benzamidine was analyzed for the signal intensity of the ligand. For the signal intensity of the protein, the selectively enhanced trypsin resonance at approximately 1.2 ppm is analyzed in the DNP method. The apparent relaxation rate of ligand (r_L) is 0.203±0.029 s^{-1}. The average value of σ_{DNP} and r_P evaluated from the DNP-NMR experiments based on six experiments using D_2O solvent is -0.097±0.014 s^{-1} and 2.413±0.644 s^{-1} respectively as

shown in table 3. The average value of σ_{DNP} and r_P obtained using H_2O solvent is -0.073±0.013 s^{-1} and 2.803±0.284 s^{-1} shown in table 4.

σ_{DNP} (-0.097 s^{-1}) obtained using D_2O solvent shown in table 3 is larger than σ_{DNP} (-0.073 s^{-1}) in H_2O solvent condition shown in table 4. The viscosity effect appears to play a role for the difference in the two σ_{DNP} values obtained with H_2O and D_2O solvent conditions.

3.5 Evaluation of the cross-relaxation rate (σ_{DNP}) in DNP-NMR

Signal buildup and decay of the protein and ligand towards Boltzmann's equilibrium was analyzed. Time-resolved signal intensity data provided a good fit with the model equations indicating that signal is transferred via NOE from the hyperpolarized ligand to the protein. That entailed determination of the fit parameters including the cross-relaxation rate (σ_{DNP}) between the protein and the ligand from the model equation.

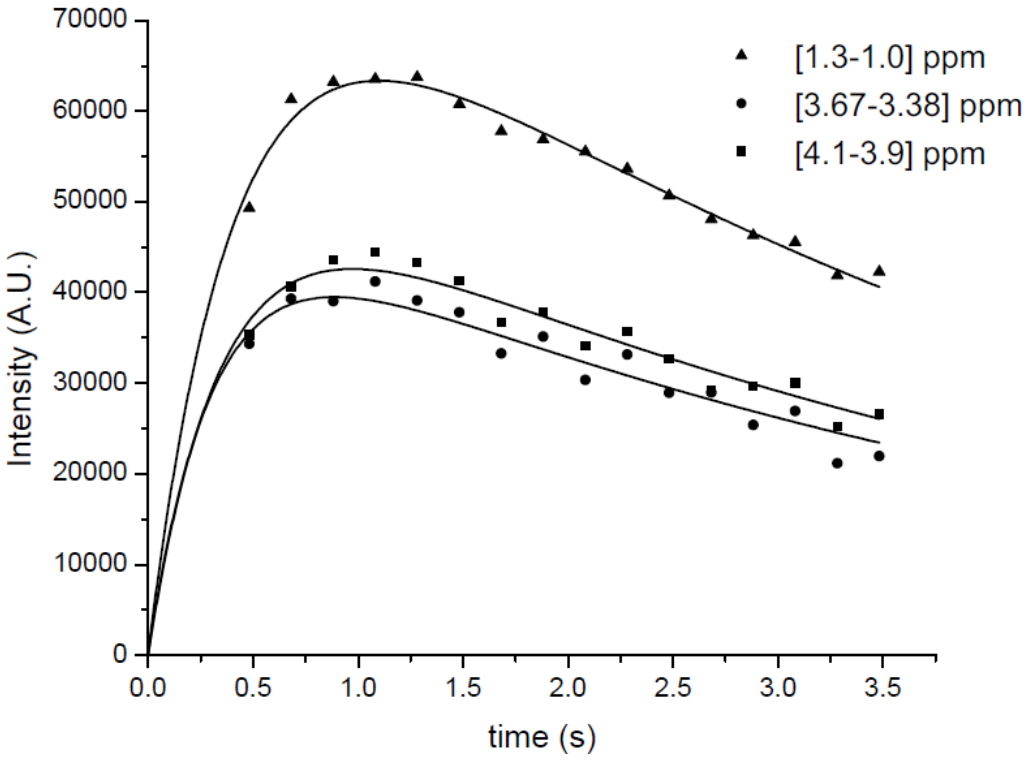

Figure 11. Proton signal build-up for different enhanced peaks. [1.2 ppm (σ_{DNP}= -0.114 s^{-1}, r_P= 2.34 s^{-1}), 3.55 ppm (σ_{DNP}= -0.089 s^{-1}, r_P= 2.79 s^{-1}), 4 ppm (σ_{DNP}= -0.092 s^{-1}, r_P= 3.19 s^{-1})]. r_P is the apparent relaxation rate of the protein used in the DNP model equations explained in section 3.4.

Figure 11 shows that different spins generate the maximum signal at approximately 1.2 s. Beyond the maximum signal, their signal intensities decrease at a longer time. The purpose of this analysis was to extract information about the cross-relaxation rate (σ_{DNP}) and an apparent relaxation rate (r_P) for each enhanced peak. The fit parameters, the cross-relaxation rate (σ_{DNP}) and the apparent relaxation rate of the protein (r_p), were evaluated using the two equations (III.1) and (III.2) shown in section

3.4 and determined to be (-0.114 s^{-1}, 2.34 s^{-1}), (-0.089 s^{-1}, 2.79 s^{-1}) and (-0.092 s^{-1}, 3.19 s^{-1}) for each resonance 1.2 ppm, 3.55 ppm and 4 ppm, respectively. Those values were obtained from one experiment (Experiment # 3121) shown in table 3.

The comparison of the cross-relaxation rates (σ_{DNP}) shows similar values for different selectively enhanced peaks. The transferred polarization signals of different protein proton spins reach the maximum approximately at 1 s from the time of the initial contact between the protein and the hyperpolarized ligand discussed in section 3.4. At the maximum, the rate of polarization signal transferred to the protein equals the rate of loss of the polarization signal of the protein due to its spin relaxation. It can also be noted in the figure that the polarization signals of different protein spins decay approximately at similar rates.

3.6 Analysis of STD-NMR data

In the STD-NMR method, the cross-relaxation rate (σ_{STD}) obtained from STD-NMR is evaluated to be compared with σ_{DNP}. STD exploits the steady-state Nuclear Overhauser Effect (NOE) which is the transfer of magnetization (M_z) (to be specific "saturation") from the perturbed spin (protein proton spin) to another spin (ligand proton spin) through dipolar interaction.[10] The equation defining the saturation transfer difference amplification factor (STD-AF) can be expressed as[3]:

$$STD - AF_o = \alpha_{STD} \frac{[L]}{[L] + K_D} \qquad \text{(IV.1)}$$

The free ligand concentration [L] can be approximated as the total ligand concentration [L_t], since the concentration of the bound ligand is much smaller than that of the free

ligand for the typical range of ligand concentrations used in STD experiments. The equation (IV.1) enables determination of two fit parameters (α_{STD}) and (K_D) from STD-NMR titration experiments using different concentrations of ligand for a fixed concentration of protein.[2] α_{STD} represents the maximum STD-AF when all the protein molecule are saturated with the ligand at an infinite ligand concentration (i.e. $\frac{[L]}{[L]+K_D} = \frac{[PL]}{[P]+[PL]}$ which is the fraction of protein bound to the ligand approaches 1). K_D represents the dissociation constant.

The general Solomon equations describing the evolution of perturbed spin towards equilibrium assume that the two spins are always bound. Equations (IV.2 and IV.3) describe the Solomon equations in the idealized case in which one protein spin and one ligand spin only is assumed and the two spins are assumed to be in either free or bound state. The populations of free and bound state are dictated by the kinetic exchange equilibrium. The equations (IV.2) and (IV.3) can be readily applied for the two spin system involving kinetic exchange as in the case of the protein and ligand spin system. The equations describing the evolution of the magnetization of the bound ligand (I_{Lb}) and the free ligand (I_{Lf}) with consideration of the kinetic exchange (k_{off} and k_{on}) between the protein and the ligand can be expressed as: [42,58]

$$\frac{dI_{Lb}}{dt} = \rho_{Lb} I_{0Lb} - (k_{off} + \rho_{Lb}) I_{Lb} + k_{on} I_{Lf} + q I_{0Pb} \qquad \text{(IV.2)}$$

$$\frac{dI_{Lf}}{dt} = \rho_{Lf} I_{0Lf} - (k_{on}[P] + \rho_{Lf}) I_{Lf} + k_{off} I_{Lb} \qquad \text{(IV.3)}$$

ρ_{Lb} and ρ_{Lf} represent the relaxation rate ($1/T_1$) of the bound ligand and free ligand. I_{0Eb} is the magnetization of the protein at the Boltzmann thermal equilibrium. The symbols (I) designated with the subscript (0) indicate the z-magnetization at the Boltzmann equilibrium. I_{0Lf} and I_{Lf} represent the off-resonance and on-resonance signal intensities of the free ligand. Off-resonance (reference) condition refers to the Boltzmann Equilibrium. It can be noted that the notation (I_o) used earlier for the off-resonance ligand signal intensity represents the cumulative ligand signal intensity (I_{0Lf}+I_{0Lb}). Similarly, the on-resonance ligand signal intensity (I) represents the cumulative on-resonance intensity (I_{Lf}+I_{Lb}). I_{0Pb} symbolizes the on-resonance bound protein signal intensity. The fractional intensity change in the free ligand (I_{0Lf}−I_{Lf}/I_{0Lf}) on saturation of protein was shown to be proportional to the cross-relaxation rate with the approximation of high ligand excess and the assumption that the off-rate is much faster than the relaxation rate of the bound ligand. The chemical exchange rates, k_{off} and k_{on}, are defined as the off-rate constant (rate of dissociation of the bound state (PL)) and the on-rate constant (rate of association of the free states (P) and (L)) according to the association/dissociation equilibrium. q is defined as transferred magnetization rate which is the summation over the whole protein of the protein-ligand cross-relaxation (σ) multiplied with the fractional saturation of the protein protons (f_{Pb}) (i.e. q=-$\sum\sigma_{PL}$ f_{Pb}) where f_{Pb}=((I-I_o)/I_o) and σ_{PL} is the cross-relaxation term between a protein spin and a ligand spin.

Solving the above coupled differential equations at the steady state condition with the assumption that the concentration of the free ligand is much larger than that of

the bound ligand generates the following equation (IV.4) (shown in the supporting information of the literature[42]).

$$I_{Lf} - I_{0Lf} = \frac{qI_{0Pb}}{\rho_{Lf}} \qquad \text{(IV.4)}$$

In our case, we only consider the protein spins that are fully saturated so that f_{Pb}= -1. In addition, we assume all the saturated protein spins as one spin and all saturated ligand spins as one spin so that we use the cross-relaxation term (σ) between the two interacting spins so that q=σ I_{0Pb} represents the thermal equilibrium spin population of the bound protein. Rearranging the equation (IV.4) with (I_{0Pb}/I_{0Lf}=$[PL]/[L_t]$) and $[PL] \approx \frac{[L]_t[P]_t}{K_D + [L]_t}$, and incorporation of additional assumptions described above gives:[42]

$$STD - AF_{\max} = \frac{I_{0Lf} - I_{Lf}}{I_{0Lf}} \frac{[L]_t}{[P]_t} = -\frac{\sigma'}{\rho_{Lf}} \left(\frac{[L]}{[L] + K_D} \right) \qquad \text{(IV.5)}$$

I_o and I shown in (IV.1) can be approximated as I_{0Lf} and I_{Lf} since the free ligand population is much larger than the bound ligand concentrations in STD experiments. Similarly, the experimental $[L]_t$ value is approximately used for $[L]$. The relaxation rate of the free ligand (ρ_{Lf}) can be determined from an independent inversion-recovery experiment.[2]

$$STD - AF_{\max,el} = \frac{I_{0Lf} - I_{Lf}}{I_{0Lf}} \frac{[L]_t}{[P]_t} = -\frac{\sigma_{STD}}{\rho_{Lf}} \qquad \text{(IV.6)}$$

At an excess ligand concentration, the equation (IV.5) can be expressed as the equation (IV.6). The maximum STD-AF signal ($STD\text{-}AF_{max,el}$) obtained at the saturation equilibrium condition and an excess ligand concentration shown in (IV.6) represents the

parameter σ_{STD} divided by the relaxation rate of the free ligand (ρ_{Lf}). The saturation equilibrium is reached after a sufficient protein saturation time is employed (~5 times T_1).

3.7 Determination of spin-lattice relaxation time (T_1)

The inversion-recovery experiment was performed to evaluate ρ_{Lf} ($1/T_1$) necessary for the analysis of STD-NMR data. The initial state of the spins was created by a 180° hard pulse followed by a variable delay time (τ) during which the z-magnetization recovers from 180°. Subsequently, a 90° pulse was applied to measure the z-magnetization (M_z). The pulse sequence is repeated using an incremental delay time (τ). [59–61]

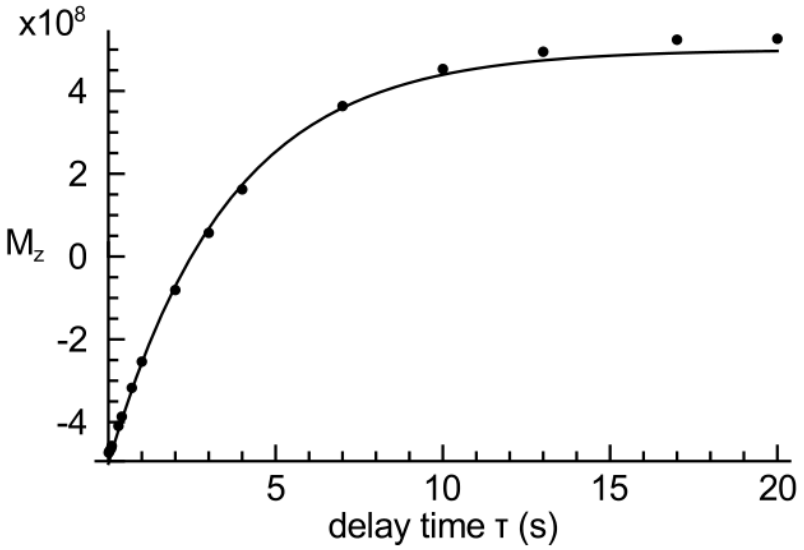

Figure 12. Determination of T_1(s) for pure benzamidine in H_2O solvent. The plot of intensity of benzamidine aromatic ring proton resonance representing M_z as a function of the time delay (τ). $M_z = M_o \cdot (1-2\exp(-\tau/T_1))$ is used to determine the fit parameters T_1 and M_o.

T_1 for pure benzamidine in H_2O solvent is evaluated to be 3.57 s from the inversion-recovery experiment shown in figure 12.

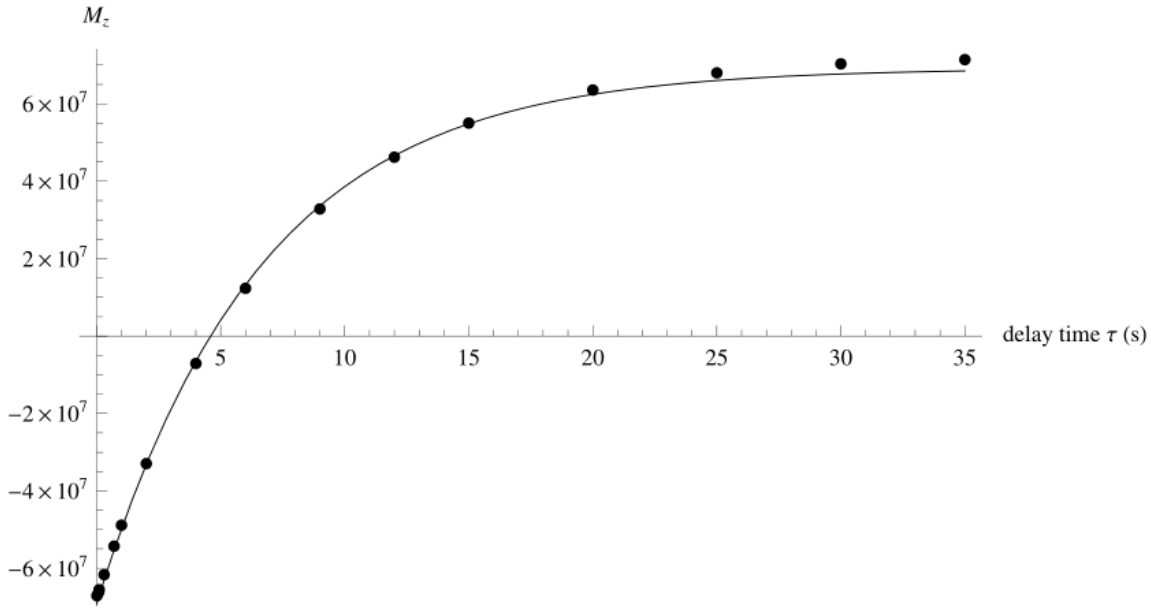

Figure 13. Determination of T_1(s) for pure benzamidine in D_2O solvent. The plot of intensity of benzamidine aromatic ring proton resonance representing M_z as a function of the time delay (τ). $M_z = M_o \cdot (1-2\exp(-\tau/T_1))$ is used to determine the fit parameters T_1 and M_o.

T_1 for pure benzamidine in D_2O solvent is evaluated to be 6.62 s from the inversion-recovery experiment shown in figure 13.

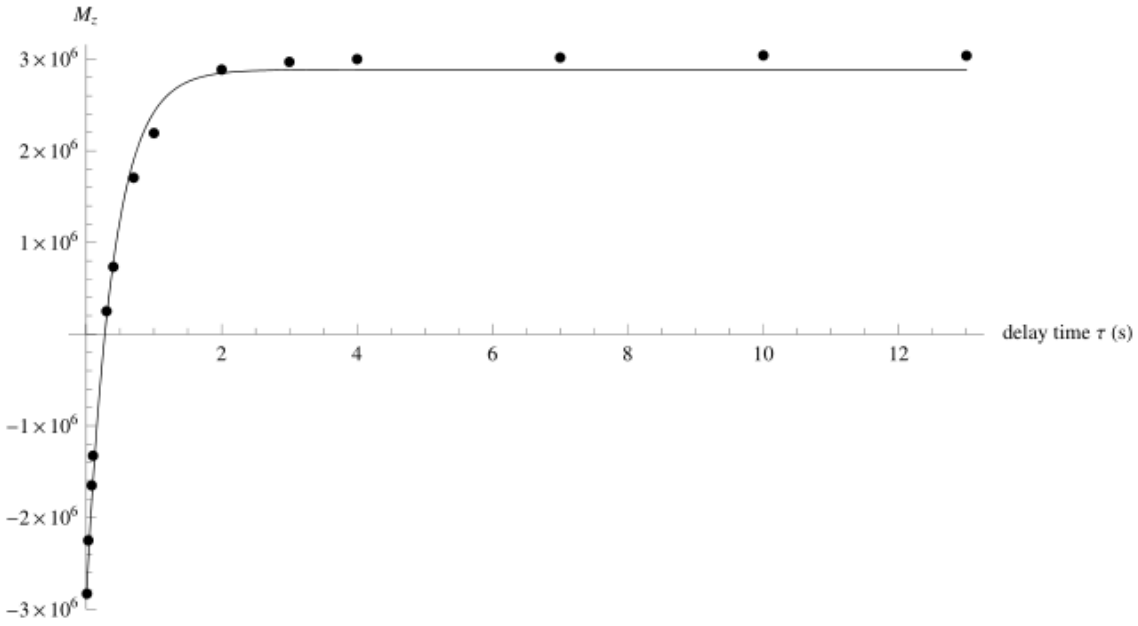

Figure 14. Determination of T_1(s) for trypsin in H_2O solvent. Trypsin (1 mM) with benzamidine (10 mM) sample in pure H_2O solvent. T_1 for the trypsin peak (i.e. the spins within the range [1.11 ppm-1.22 ppm]) representative of the polarized spins in the DNP-NMR was evaluated to be 0.40 s.

T_1 for pure benzamidine in H_2O solvent is evaluated to be 0.40 s from the inversion-recovery experiment shown in figure 14.

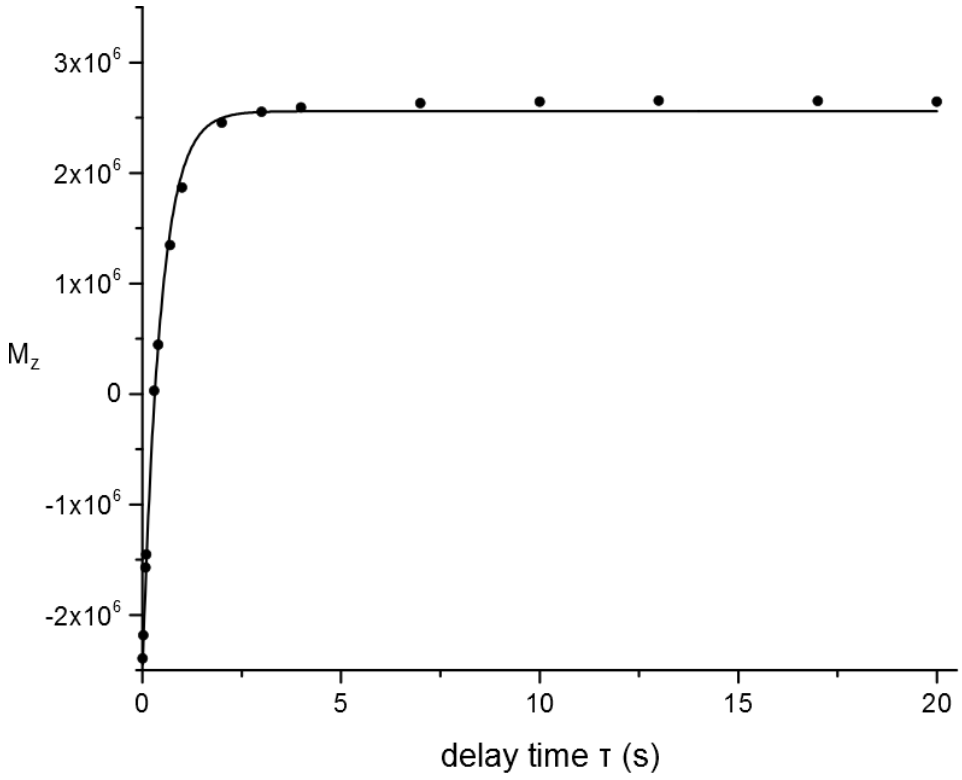

Figure 15. Determination of T_1(s) for trypsin in D_2O solvent. Trypsin (1 mM) with benzamidine (10 mM) sample in pure D_2O solvent.

T_1 for the trypsin peak (i.e. the spins within the range [1.11 ppm-1.22 ppm]) representative of the polarized spins in the DNP-NMR was measured in the inversion-recovery experiment shown in figure 15. T_1 for pure benzamidine in D_2O solvent is evaluated to be 0.45 s.

3.8 Evaluation of the cross-relaxation rate (σ_{STD}) in STD-NMR

STD-AF value is influenced by the saturation time. In the case of a long saturation time, a ligand molecule that has already received saturation via its interaction with the saturated protein can rebind to the same or another protein molecule. The

macroscopic STD-AF signal can be underestimated due to the rebinding process at long saturation times. The saturated ligand molecules receive significantly less saturation upon re-binding than upon binding the first time.

The determination of the initial growth rates from the plot of STD-AF as a function of saturation time using the equation (V.1) can be used to obtain the corrected STD values ($STD\text{-}AF_o$) for each ligand concentration.[47,62] The slope method yields an accurate signal build-up information by only accounting for the STD signal buildup at early saturation times when there are many unsaturated free ligand molecules to bind to saturated protein molecules. It is also applied for removing the different T_1 biases arising from each individual proton spin within a particular ligand to give the STD values representative of the proximity of each proton spin to the protein spin.[48,63]

$$STD\text{-}AF(t_{sat}) = STD\text{-}AF_{\max}[1 - \exp(-k_{sat}t_{sat})] \qquad \text{(V.1)}$$

$STD\text{-}AF_{max}$ and k_{sat} in the equation (V.1)[43,48] were also denoted as (σ/ρ) and ρ respectively in the supporting information section of the literature[1], where σ is an apparent cross-relaxation rate and ρ is an apparent relaxation rate. σ and ρ are dependent upon concentration of the sample.

Different saturation times (t_{sat}) (1, 3, 5, 10, 20 s) were used to construct STD buildup curves and obtain the slope for each benzamidine concentration using a fixed trypsin concentration of 15.7 μM. Fitting of the equation (V.1) generates k_{sat} and $STD\text{-}AF_{max}$ for each ligand concentration.

Figure 16. The binding isotherm of STD-AF initial growth rates method. (a) shows the growth rates of STD-AF as a function of saturation times using a fixed trypsin concentration of 15.7 μM. (b) For each ligand concentration, the buildup curve is fitted with the analogous form of the equation (V.1) to obtain the initial slopes, $STD\text{-}AF_o$, (c) These initial slope values ($STD\text{-}AF_o$) are plotted as a function of benzamidine concentration to generate a Langmuir isotherm from which $STD\text{-}AF^{o}_{max}$= 0.395 s^{-1} and K_D= 81 μM were evaluated using the analogous form of the equation (IV.1) where $STD\text{-}AF^{o}_{max}$ represents the initial slope at an excess ligand concentration. Note: The same stock solutions of trypsin and benzamidine were used to prepare the solutions of trypsin and benzamidine solution mixture for each measurement in this STD-NMR protein-ligand titration experiment. The exact concentration in the stock solutions was determined with UV spectrophotometry.

(a)

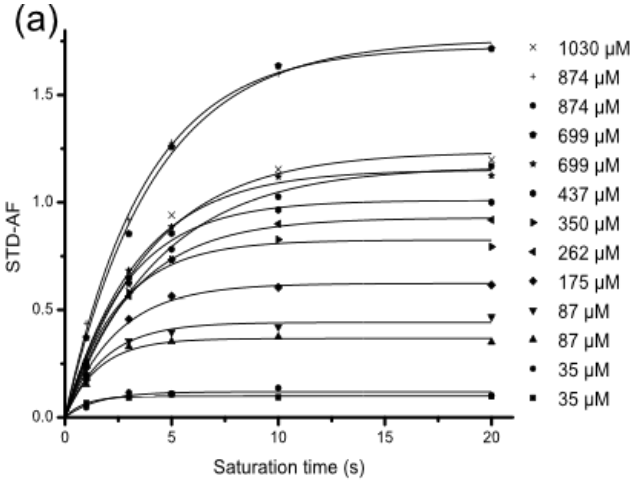

(b)

Benzamidine concentration [µM]	STD-AF_{max}	k_{sat} [s^{-1}]	STD-AF_o (STD-AF_{max} * k_{sat})
35	0.099	1.071	0.106
35	0.119	0.640	0.076
87	0.367	0.624	0.229
87	0.442	0.530	0.234
175	0.622	0.414	0.258
262	0.928	0.314	0.291
350	0.825	0.395	0.326
437	1.010	0.338	0.341
699	1.152	0.294	0.339
699	1.758	0.240	0.422
874	1.167	0.228	0.266
874	1.723	0.266	0.458
1030	1.235	0.250	0.309

(c)

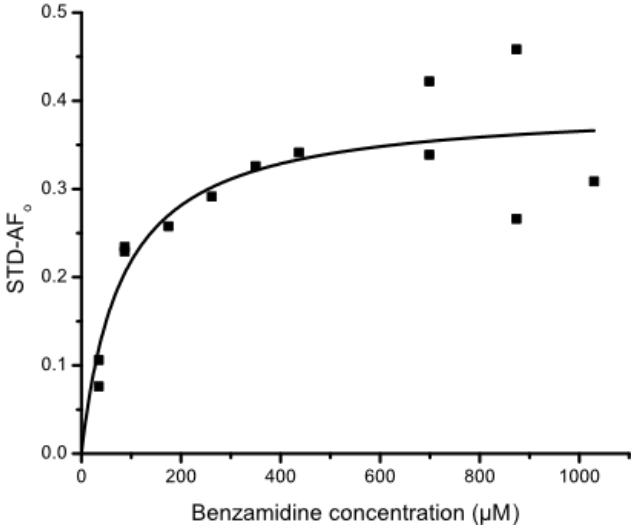

Plotting the $STD\text{-}AF_o$ values from the slope ($STD\text{-}AF_{max}\ k_{sat}$) as a function of each ligand concentration generates a Langmuir hyperbolic curve which can be fitted with the equation using the approximation that the total ligand concentration $[L]_o$ is equal to free ligand concentration $[L]$.

The experimental data from the STD-NMR experiment exhibits a significant error at high ligand concentrations due to the very weak intrinsic STD signal at high ligand concentrations.

Table 5. The fit parameters evaluated from STD-NMR

K_D (μM)	$STD\text{-}AF^o_{max}$ (s^{-1})
81	0.395

As shown in table 5, $STD\text{-}AF^o_{max}$ was determined to be 0.395 s^{-1} using the equation (IV.1). $STD\text{-}AF^o_{max}$ from the slope method can be compared to $-\sigma_{STD}$ obtained from ($STD\text{-}AF_{max,el}\rho_{Lf}$) shown in equation (IV.6) if the protein saturation buildup reached the steady state immediately following the saturation.

3.9 Determination of K_D with Isometric Calorimetric Titration (ICT)

Isothermal Calorimetric Titration (ICT) method was employed to independently determine K_D and compare it with K_D obtained from the STD-NMR method as a way to ensure the reliability of the STD-NMR method. Titration of trypsin with benzamidine was carried out using Tris buffer containing 10 mM $CaCl_2$ at pH 7.0 and 25^o C. The data (K) represents the association equilibrium constant (i.e. $1/K_D$). K_D is determined to be 45.2 μM which is comparable to (81 μM) obtained from the STD-NMR method.

According to the literatures,[8–11] the K_D values evaluated from a variety of methods and instruments typically vary approximately from 18 μM to 150 μM with different experimental conditions such as the type of buffer, concentration of buffer, salt concentration and pH. The K_D value is consistent with those reported in the literature[8–10,59] and the ITC method suggests the reliability of the results from the STD method.

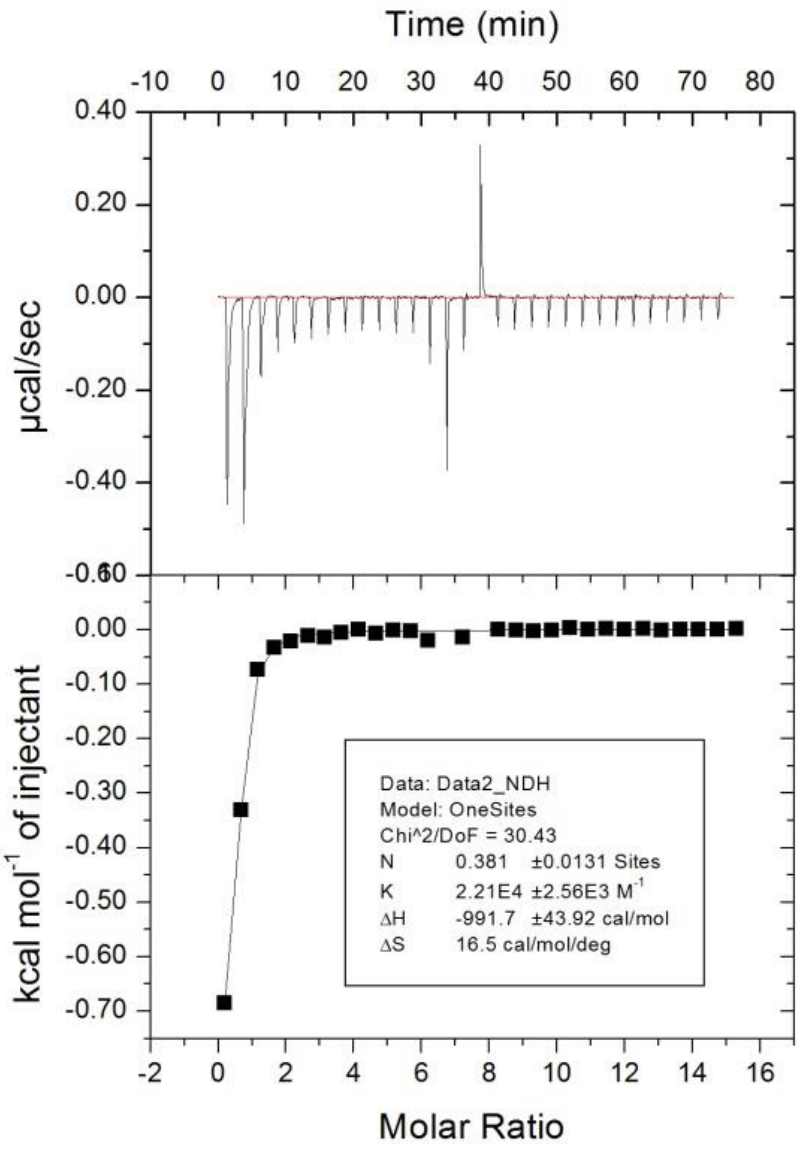

Figure 17. Determination of K_D with ITC experiment. The top figure shows the power output (µcal/sec) to maintain the reference temperature as a function of time and the bottom figure shows the heat generated due to titration as a function of the molar ratio of total benzamidine to trypsin respectively.

3.10 Comparison between DNP-NMR and STD-NMR

The STD-NMR method is based on the steady-state NOE caused by two opposing effects. The NOE build-up of the ligand from binding with the saturated protein is counteracted by T_1 longitudinal relaxation of the spins of the saturated ligand bringing them back to the Boltzmann equilibrium.

With DNP-NMR experiments, we studied the transient phenomena associated with the longitudinal relaxation of hyperpolarized spins of the ligand, the transfer of magnetization from the ligand to the protein and the longitudinal relaxation of the transferred signal back to the Boltzmann equilibrium.

In both the DNP-NMR and STD-NMR method applied in this study, the cross-relaxation rate (σ_{DNP} or σ_{STD}) represents an average σ value between a group of spins (approximated as one spin based on the models) at the binding pocket and a group of ligand spins (approximated as one spin based on the models).

Hyperpolarization with DNP enables the generation of sufficient signal with a single scan. With the DNP-NMR method, σ_{DNP} can be obtained in a single experiment which takes as little as 5 s of the NMR measurement time.

4. SUMMARY AND CONCLUSION

In this study, we attempted to probe the protein binding pocket by investigating the transfer of polarization from the ligand to the protein binding pocket.

DNP-NMR experiments showed that the polarization signal of the hyperpolarized ligand transferred to the protein, specifically the protein binding pocket region. The non-uniform signal enhancement of the protein resonances suggests that the protein region where the hyperpolarized ligand binds to may be selectively polarized. Previous research on the polarization transfer from the protein ligand binding interaction was concerned with mapping the ligand epitope via analysis of the enhanced ligand proton signals.[29] Although recent research on the spectral analysis was performed with hyperpolarized small protein or peptides, the observed protein NMR signals of the hyperpolarized proteins were directly amplified thermal NMR signals of the proteins themselves.[64] This study was focused on analysis of the selectively enhanced signals of a protein, trypsin, that receives polarization from interacting with the hyperpolarized ligand.

The comparison of the selectively enhanced protein spectra (a single scan) obtained from DNP-NMR experiment with the STD ligand spectra constructed from a set of STD-NMR measurements across the wide range of frequencies suggests that the two experiments were symmetrical. The symmetry of the two experiments was expected, since in DNP-NMR, the polarization signal transfers from the hyperpolarized ligand to the protein binding site, whereas the saturation signal transfers from the protein binding site to the ligand in STD-NMR. DNP-NMR spectra obtained from the single scan show a

much higher signal resolution and require less time (a few seconds of measurement time after 30 minutes of hyperpolarization period) compared to the STD ligand spectra, which typically require from at least a day to several days for scanning saturation frequency.

Model equations were used to mathematically describe the process of polarization signal transfer from the ligand to the protein. The cross-relaxation rate (σ) was evaluated by fitting the model equations into experimental data, the selectively enhanced signal intensity of the protein and the signal intensity of hyperpolarized ligand as a way to obtain a quantitative measurement of signal transfer. The σ_{DNP} value (-0.073±0.013 s^{-1}) evaluated from the DNP-NMR method. $STD\text{-}AF^{o}_{max}$ from the slope method could approximately represent $-\sigma_{STD}$ obtained from ($STD\text{-}AF_{max,el,\rho_{Lf}}$) if the protein saturation buildup reached the steady state immediately following the saturation. In such a case, the σ_{STD} value would be on the order of -0.4 s^{-1}. The influence of the relaxation of polarized spins due to dipolar interaction with other nearby spins within the protein could play a role in defining the numerical values. However, additional theoretical work may yield a more precise interpretation of these parameters.

Another fit parameter K_D evaluated from the STD-NMR method (81 μM) was compared with the K_D value (45.2 μM) obtained from an independent ITC method and the two K_D values were shown to be in reasonable agreement, suggesting that the experimental data obtained with STD-NMR method is reliable.

The NMR spectrum of the trypsin in the DNP-NMR spectrum after polarization transfer from hyperpolarized ligand is different from the non-hyperpolarized spectrum of trypsin. Trypsin peaks are selectively enhanced at approximately 4 ppm, 3.6 ppm, 3.3

ppm, 1.2 ppm and -0.8 ppm. It can be inferred from this experimental observation that the enhanced trypsin signals represent the signal enhancement of the amino acid residues located in the protein binding pocket. Therefore, the present work may in the future be extended for the detailed structural identification of the protein binding pocket.[3]

REFERENCES

1. Mizukoshi, Y. *et al.* An accurate pharmacophore mapping method by NMR spectroscopy. *Angew. Chem.-Int. Ed.* **51,** 1362–1365 (2012).
2. Dalvit, C. *et al.* Identification of compounds with binding affinity to proteins via magnetization transfer from bulk water. *J. Biomol. NMR* **18,** 65–68 (2000).
3. Peng, J. W., Moore, J. & Abdul-Manan, N. NMR experiments for lead generation in drug discovery. *Prog. Nucl. Magn. Reson. Spectrosc.* **44,** 225–256 (2004).
4. Meyer, B. & Peters, T. NMR Spectroscopy techniques for screening and identifying ligand binding to protein receptors. *Angew. Chem. Int. Ed.* **42,** 864–890 (2003).
5. Chen, A. & Shapiro, M. J. NOE Pumping: A novel NMR technique for identification of compounds with binding affinity to macromolecules. *J. Am. Chem. Soc.* **120,** 10258–10259 (1998).
6. Pellecchia, M. *et al.* Perspectives on NMR in drug discovery: a technique comes of age. *Nat. Rev. Drug Discov.* **7,** 738–745 (2008).
7. Mandal, P. K. *et al.* Towards a structural basis for the relationship between blood group and the severity of El Tor Cholera. *Angew. Chem. Int. Ed.* **51,** 5143–5146 (2012).
8. Talhout, R. & Engberts, J. B. Thermodynamic analysis of binding of p-substituted benzamidines to trypsin. *Eur. J. Biochem. FEBS* **268,** 1554–1560 (2001).
9. Sun, J., Kitova, E. N. & Klassen, J. S. Method for stabilizing protein−ligand complexes in nanoelectrospray ionization mass spectrometry. *Anal. Chem.* **79,** 416–425 (2007).

10. Clark, S. M. & Konermann, L. Determination of ligand−protein dissociation constants by electrospray mass spectrometry-based diffusion measurements. *Anal. Chem.* **76,** 7077–7083 (2004).
11. Maresgui.m & Shaw, E. Studies on active center of trypsin - binding of amidines and guanidines. *J. Biol. Chem.* **240,** 1579–& (1965).
12. Krieger, M., Kay, L. M. & Stroud, R. M. Structure and specific binding of trypsin: Comparison of inhibited derivatives and a model for substrate binding. *J. Mol. Biol.* **83,** 209–230 (1974).
13. Duong-Thi, M.-D. *et al.* Weak affinity chromatography as a new approach for fragment screening in drug discovery. *Anal. Biochem.* **414,** 138–146 (2011).
14. Buch, I., Giorgino, T. & Fabritiis, G. D. Complete reconstruction of an enzyme-inhibitor binding process by molecular dynamics simulations. *Proc. Natl. Acad. Sci.* **108,** 10184–10189 (2011).
15. Pereira, M. T., Silva-Alves, J. M., Martins-Jose, A., Lopes, J. C. D. & Santoro, M. M. Thermodynamic evaluation and modeling of proton and water exchange associated with benzamidine and berenil binding to beta-trypsin. *Braz. J. Med. Biol. Res.* **38,** 1593–1601 (2005).
16. Ernst, R. R. & Anderson, W. A. Application of fourier transform spectroscopy to magnetic resonance. *Rev. Sci. Instrum.* **37,** 93–102 (1966).
17. Matsumoto, S. *et al.* Generation of 24 T at 4.2 K using a layer-wound GdBCO insert coil with Nb3Sn and Nb-Ti external magnetic field coils. *Supercond. Sci. Technol.* **25,** 025017 (2012).

18. Hore, P. & Broadhurst, R. Photo-Cidnp of Biopolymers. *Prog. Nucl. Magn. Reson. Spectrosc.* **25,** 345–402 (1993).

19. Walker, T. G. & Happer, W. Spin-exchange optical pumping of noble-gas nuclei. *Rev. Mod. Phys.* **69,** 629–642 (1997).

20. Natterer, J. & Bargon, J. Parahydrogen induced polarization. *Prog. Nucl. Magn. Reson. Spectrosc.* **31,** 293–315 (1997).

21. Duckett, S. B. & Sleigh, C. J. Applications of the parahydrogen phenomenon: A chemical perspective. *Prog. Nucl. Magn. Reson. Spectrosc.* **34,** 71–92 (1999).

22. Ardenkjaer-Larsen, J. H. *et al.* Increase in signal-to-noise ratio of > 10,000 times in liquid-state NMR. *Proc. Natl. Acad. Sci. U. S. A.* **100,** 10158–10163 (2003).

23. Prisner, T. F. in *NMR Biomol.* (Bertini, I., McGreevy, K. S. & Parigi, G.) 419–431 (Wiley-VCH Verlag GmbH & Co. KGaA, 2012). at <http://onlinelibrary.wiley.com/doi/10.1002/9783527644506.ch25/summary>

24. Abragam, A. & Goldman, M. Principles of dynamic nuclear-polarization. *Rep. Prog. Phys.* **41,** 395–467 (1978).

25. Mieville, P., Jannin, S., Helm, L. & Bodenhausen, G. NMR of insensitive nuclei enhanced by dynamic nuclear polarization. *Chimia* **65,** 260–263 (2011).

26. Barnes, A. B. *et al.* High-field dynamic nuclear polarization for solid and solution biological NMR. *Appl. Magn. Reson.* **34,** 237–263 (2008).

27. Hilty, C. & Bowen, S. Applications of dynamic nuclear polarization to the study of reactions and reagents in organic and biomolecular chemistry. *Org. Biomol. Chem.* **8,** 3361–3365 (2010).

28. Bowen, S. & Hilty, C. Rapid sample injection for hyperpolarized NMR spectroscopy. *Phys. Chem. Chem. Phys.* **12,** 5766–5770 (2010).

29. Lee, Y. *et al.* Hyperpolarized binding pocket nuclear overhauser effect for determination of competitive ligand binding. *Angew. Chem.-Int. Ed.* **51,** 5179–5182 (2012).

30. Lee, Y., Heo, G. S., Zeng, H., Wooley, K. L. & Hilty, C. Detection of living anionic species in polymerization reactions using hyperpolarized NMR. *J. Am. Chem. Soc.* **135,** 4636–4639 (2013).

31. Ragavan, M., Chen, H.-Y., Sekar, G. & Hilty, C. Solution NMR of polypeptides hyperpolarized by dynamic nuclear polarization. *Anal. Chem.* **83,** 6054–6059 (2011).

32. Mo, H. P. & Pochapsky, T. C. Intermolecular interactions characterized by nuclear Overhauser effects. *Prog. Nucl. Magn. Reson. Spectrosc.* **30,** 1–38 (1997).

33. Netzel, D. & Miknis, F. Nuclear-spin relaxation spectroscopy. *Appl. Spectrosc.* **31,** 365–386 (1977).

34. Clore, G. M. & Gronenborn, A. M. Theory of the time dependent transferred nuclear Overhauser effect: Applications to structural analysis of ligand-protein complexes in solution. *J. Magn. Reson. 1969* **53,** 423–442 (1983).

35. Ni, F. Recent developments in transferred NOE methods. *Prog. Nucl. Magn. Reson. Spectrosc.* **26, Part 6,** 517–606 (1994).

36. Mo, H. & Pochapsky, T. C. Intermolecular interactions characterized by nuclear Overhauser effects. *Prog. Nucl. Magn. Reson. Spectrosc.* **30,** 1–38 (1997).

37. Zerbe, O. & Jurt, S. *Applied NMR Spectroscopy for Chemists and Life Scientists*. (John Wiley & Sons, 2013).

38. Kowalewski, J. & Maler, L. *Nuclear Spin Relaxation in Liquids: Theory, Experiments, and Applications*. (CRC Press, 2006).

39. Boulat, B. & Bodenhausen, G. Cross relaxation in magnetic resonance: An extension of the Solomon equations for a consistent description of saturation. *J. Chem. Phys.* **97,** 6040 (1992).

40. Fielding, L. NMR methods for the determination of protein–ligand dissociation constants. *Prog. Nucl. Magn. Reson. Spectrosc.* **51,** 219–242 (2007).

41. Fielding, L., Rutherford, S. & Fletcher, D. Determination of protein–ligand binding affinity by NMR: observations from serum albumin model systems. *Magn. Reson. Chem.* **43,** 463–470 (2005).

42. Kemper, S. *et al.* Group epitope mapping considering relaxation of the ligand (GEM-CRL): Including longitudinal relaxation rates in the analysis of saturation transfer difference (STD) experiments. *J. Magn. Reson.* **203,** 1–10 (2010).

43. Angulo, J., Enríquez-Navas, P. M. & Nieto, P. M. Ligand–receptor binding affinities from Saturation Transfer Difference (STD) NMR Spectroscopy: The binding isotherm of STD initial growth rates. *Chem. – Eur. J.* **16,** 7803–7812 (2010).

44. Angulo, J. & Nieto, P. M. STD-NMR: application to transient interactions between biomolecules-a quantitative approach. *Eur. Biophys. J. Biophys. Lett.* **40,** 1357–1369 (2011).

45. Sánchez-Pedregal, V. M. *et al.* The INPHARMA Method: Protein-mediated interligand NOEs for pharmacophore mapping. *Angew. Chem. Int. Ed.* **44,** 4172–4175 (2005).

46. Ludwig, C. *et al.* SALMON: Solvent accessibility, ligand binding, and mapping of ligand orientation by NMR Spectroscopy. *J. Med. Chem.* **51,** 1–3 (2008).

47. Mayer, M. & James, T. L. NMR-based characterization of phenothiazines as a RNA binding scaffold†. *J. Am. Chem. Soc.* **126,** 4453–4460 (2004).

48. Mayer, M. & Meyer, B. Group epitope mapping by saturation transfer difference NMR to identify segments of a ligand in direct contact with a protein receptor. *J. Am. Chem. Soc.* **123,** 6108–6117 (2001).

49. Lepre, C. A., Moore, J. M. & Peng, J. W. Theory and applications of NMR-based screening in pharmaceutical research. *Chem. Rev.* **104,** 3641–3675 (2004).

50. Lepre, C. A., Moore, J. M. & Peng, J. W. Theory and applications of NMR-based screening in pharmaceutical research. *Chem. Rev.* **104,** 3641–3676 (2004).

51. Mayer, M. & Meyer, B. Characterization of ligand binding by saturation transfer difference NMR spectroscopy. *Angew. Chem.-Int. Ed.* **38,** 1784–1788 (1999).

52. Umemoto, K., Oikawa, S., Aida, M. & Sugawara, Y. Intermolecular nuclear overhauser effect and atomic pair potential approaches to wheat-germ agglutinin - sugar binding. *J. Biomol. Struct. Dyn.* **6,** 593–608 (1988).

53. Maaheimo, H., Kosma, P., Brade, L., Brade, H. & Peters, T. Mapping the binding of synthetic disaccharides representing epitopes of chlamydial lipopolysaccharide to antibodies with NMR. *Biochemistry (Mosc.)* **39,** 12778–12788 (2000).

54. Zeng, H., Lee, Y. & Hilty, C. Quantitative rate determination by dynamic nuclear polarization enhanced NMR of a Diels−Alder reaction. *Anal. Chem.* **82,** 8897–8902 (2010).

55. Weiz, A. R. *et al.* Harnessing the evolvability of tricyclic microviridins to dissect protease–inhibitor interactions. *Angew. Chem. Int. Ed.* **53,** 3735–3738 (2014).

56. Vulpetti, A., Hommel, U., Landrum, G., Lewis, R. & Dalvit, C. Design and NMR-based screening of LEF, a library of chemical fragments with different local environment of fluorine. *J. Am. Chem. Soc.* **131,** 12949–12959 (2009).

57. Zeng, H. Quantitative determination of chemical processes by dynamic nuclear polarization enhanced nuclear magnetic resonance spectroscopy. (2012).

58. Clore, G. M. & Gronenborn, A. M. Theory and applications of the transferred nuclear overhauser effect to the study of the conformations of small ligands bound to proteins. *J. Magn. Reson. 1969* **48,** 402–417 (1982).

59. Vold, R. L., Waugh, J. S., Klein, M. P. & Phelps, D. E. Measurement of spin relaxation in complex systems. *J. Chem. Phys.* **48,** 3831–3832 (2003).

60. Kay, L., Torchia, D. & Bax, A. backbone dynamics of proteins as studied by N-15 inverse detected heteronuclear NMR-spectroscopy - application to Staphylococcal nuclease. *Biochemistry (Mosc.)* **28,** 8972–8979 (1989).

61. Sklenar, V., Torchia, D. & Bax, A. measurement of C-13 longitudinal relaxation using H-1 detection. *J. Magn. Reson.* **73,** 375–379 (1987).

62. Angulo, J. *et al.* Saturation Transfer Difference (STD) NMR spectroscopy characterization of dual binding mode of a mannose disaccharide to DC-SIGN. *Chembiochem* **9,** 2225–2227 (2008).

63. Mayer, M. & James, T. L. NMR-based characterization of phenothiazines as a RNA binding scaffold. *J. Am. Chem. Soc.* **126,** 4453–4460 (2004).

64. Ragavan, M., Chen, H.-Y., Sekar, G. & Hilty, C. Solution NMR of polypeptides hyperpolarized by dynamic nuclear polarization. *Anal. Chem.* **83,** 6054–6059 (2011).